UNIVERSITÀ DEGLI STUDI DI PADOVA

UNIVERSITÁ DEGLI STUDI DI PADOVA
Dipartimento di Ingegneria Industriale DII
Corso di Laurea Magistrale in Ingegneria Aerospaziale

Validation of the noise prediction code Rnoise and reduction of trailing edge noise by Active Flow Control

Thesis coordinators:
Mohammad Kamruzzaman, Alexander Wolf [1]
Ernesto Benini [2]

Author:
Davide Matera
matr. 1012970

Anno Accademico 2012/2013

[1]Universität Stuttgart
[2]Università degli Studi di Padova

Thanks to everyone i met and stumbled on during my beautiful stay in Germany. Thanks to who hosted, teached, scolded, accompained me in this period, i will not forget you.

Grazie a tutti coloro che ho conosciuto e incontrato durante la mia fantastica permanenza in Germania. Grazie a coloro che mi hanno ospitato, istruito, rimproverato e accompagnato in questo periodo, non vi dimenticherò.

Summary

This thesis focuses on the problem of Trailing-Edge (TE) noise originated by airfoils subjected to a bidimensional low Mach number air flow.
Among the many observable mechanisms of noise generation from wind turbines in this flow regime, the dominant one is the boundary-layer induced trailing-edge interaction (TBL-TE) noise, which is noise of broadband type. This has been observed and proved by field tests (Oerlemans et al. [32]). This is a major concern in the aeroacoustics research field, as it occurs in many aerodynamic applications: mainly in wind turbines, but also on airframes with sharp lifting surfaces, turbomachinery, etc. The mechanisms of this kind of noise originates from the turbulent phenomena in the boundary layer, the latter presenting inhomogeneous and anisotropic characteristics and thus very difficult to model numerically.
Therefore, a reliable tool capable of predicting correctly the TBL-TE noise would be of invaluable worthiness for both industry and research purposes, being noise reduction a major concern in the aerodynamic applications which have to keep their environmental impact under control, and are in close contact with people everyday. This thesis aims to validate the noise prediction model Rnoise software in development at the IAG. The key feature of the proposed Rnoise software is that basing on CFD/RANS (time-steady) results, one can derive other turbulence parameters such as anisotropic velocity spectra, integral correlation length scales and correlation functions, which are necessary parameters for the TBL-TE noise prediction methods and are not provided from actual RANS softwares. These turbulence properties still represent a rather complex and delicate argument, and they are still being studied and deeply examinated. In addition, they can describe the anisotropy character of a turbulent boundary layer, being this necessary for a proper, accurate prediction of TBL-TE noise [4].
These modelling approaches have been already extensively validated with wind-tunnel experiments and encouraging results have been obtained [24].
After an introductory, brief presentation of the main noise scattering mechanisms, the theoretical background of the most advanced noise prediction methods available today and their foundations are presented. Afterwards, the approach used is to replicate RANS simulations of past experimental results available in the literature for various airfoils, then compare them with the Rnoise prediction which is directly fed with the RANS results. After results are analysed and discussed, the successive chapter reports how the Rnoise software is applied on RANS simulations reproducing Active Flow Control/Active Noise Control (AFC/ANC), realized trough distributed boundary-layer suction into the airfoil. It is known that trailing edge noise can be attenuated by passive devices like trailing edge serrations, and theoretical models have been already developed to predict their effect [41]. Active Noise Control devices, which are in fact a particular case of AFC, are designed to affect the turbulent motion in the boundary layer, which is already not straightforward to model by itself. An ANC device, then, benefits from all the advantages of actively controlled devices (e.g. they can be continuously regulated or shut off to match continuously the better performance requirements), and their disadvantages: energy consumption required for their operation, major weight, major complexity and thus less reliability. The aim of the AFC methodology here discussed is to reduce

the intensity of turbulence in the boundary layer along a certain portion of the suction side of an airfoil, resulting in reduced noise scattering at the trailing edge. This has been already investigated with both RANS simulations and experiments conducted at IAG on a NACA64-418 airfoil and at the University of Tel-Aviv in the Mixing Layer Facility [44], and their results, along with other informations from sources in the available literature in the field of boundary layer suction are examinated. All these informations are reported and observed in attempt to understand the results obtained in this thesis.

Contents

Nomenclature

Latin and Greek symbols

c	$[m]$	Chord length
c_0	$[ms^{-1}]$	Speed of sound
c_d	[-]	Drag coefficient
c_l	[-]	Lift coefficient
C_Q	[-]	Non-dimensional massflow, coefficient of suction
k_i	$[m^{-1}]$	Wavenumber in i-direction
k_T	$[kgm^2s^{-2}]$	Turbulent Kinetic Energy in SST and RSM turbulence models
L	$[m]$	Spanwise length of wetted trailing edge
L_p	$[dBm^{-1}]$	Sound pressure level
Q	$[kgs^{-1}]$	Suction mass flow
R	$[m]$	Noise source to receiver distance
$S(\omega)$	$[dBm^{-1}]$	Far-field noise
S_s	$[m^2]$	Suction surface
U_c	$[ms^-1]$	Mean convective velocity of wall pressure fluctuations
U_e	$[ms^-1]$	Velocity at the boundary-layer edge
U_i	$[ms^{-1}]$	Mean velocity in i-direction
u_i	$[ms^{-1}]$	Velocity fluctuation in i-direction
$\langle u_i^2 \rangle$	$[m^{-2}s^{-2}]$	Reynold stresses in i-direction
U_∞	$[ms^{-1}]$	Freestream velocity
v_s	$[ms^{-1}]$	Suction velocity
$\tilde{\Phi}_{22}$	$[m^2]$	Normalised vertical turbulence energy spectrum
Φ_m	$[s]$	Moving axis spectrum
Λ_2	$[m]$	Vertical integral length scale
μ	$[Nsm^2]$	Dynamic viscosity
ω	$[s^{-1}]$	Angular velocity
x, y, z	$[m]$	Cartesian coordinates

Subscripts, Superscripts, Abbrevations and Acronyms

AFC	Active Flow Control
ANC	Active Noise Control
BL	Boundary layer
CAA	Computational Aero-Acoustics
CFD	Computational Fluid Dynamics
exp, EXP	Experimental data
ff, FF	Far-field
IAG	Institute of Aerodynamics and Gas Dynamics
LWT	Laminar wind tunnel of the IAG
mp	Mode profile for the computation of noise sources in Rnoise code (see Sec.3.4)
ps, PS	Pressure side of the airfoil
RANS	Reynolds Averaged Navier-Stokes Equations
RMS	Root mean square
RSM	Full Reynolds stress turbulence model
SPL	Sound pressure level
ss, SS	Suction side of the airfoil
SST	Menters Shear Stress Transport two-equation turbulence model
TBL-TE	Turbulent Boundary-Layer Trailing-Edge
TE	Trailing edge
trip, clean	Forced, natural laminar-turbulent transition type

1 Introduction

This chapter introduces the reader to the problem of aeroacoustically generated noise. The following discussion is oriented to synthesize the nowadays knowledge about airfoil-generated noise with a focus on wind turbine applications.

1.1 Overview of the noise problem and motivation

The control of acoustic noise is nowadays a problem which is of high interest in every technical application worldwide. The technical progress is delivering to our daily lives machines and devices which are more and more powerful and/or performant. The noise associated with the utilization of these (cars, airplane engines, or simply air conditioners are daily observable examples), which are in close contact with our lives, needs clearly to be kept under control and government regulations are in force in every country to ensure this. The same goes for wind turbines, which are not the only prospected source of renewable energy for the future, but at least the more exploited and better proven one.
In the next years, a remarkable extension of the existing wind energy parks will be required to satisfy the current trend of energy demand and contribute to the replacing of non-renewable energy sources and ageing wind parks. The on-shore installation of wind parks has to deal with numerous problems and concerns bound to the public acceptance of their installation: among visual impact, shadowing, and noise emission the latter is a prominent matter. The perceived noise for an observer at a given location depends from many factors, namely the turbine construction, operation, and situational factors. This means, not only intuitive factors like distance and rotational speed, but also tower, tip and airfoil shape, other buildings in the vicinity, the characteristics of the noise source (i.e. tonality and impulsive character) play a role.
Furthermore, it is known that the definition of noise is not unique and objective. Noise is a personal, subjective matter and an acoustic propagation can be perceived at the same time as annoying noise for one, while being not bothering for another or even impossible to withstand for another person. Many influencing factors on the perception of noise can be physical health, personality, mood, or even personal beliefs regarding the noise source, and these aspects fall out of the bounds of the present work. To outline a common, objective regulation on noise emission in order to ensure right living conditions and protect environment, national and international institutions provide a both technical and common sense based management of the allowable sound emissions, which take account of the type of territory (rural, commercial, residential) and the time of the day.
Researching solutions to reduce remarkably noise impact of wind turbine installations could open them the path to previously inaccessible zones, making easier the development and expansion of renewable energy sources, or even freeing the way to new ideas that were previously prohibited due to the unacceptable sound emissions.

1.2 Origins of noise in a wind turbine

Noise emissions of different nature can be distinguished for a wind turbine. A minor part is *mechanically* generated noise, originated from the machinery components (gearbox, generator, cooling fans, hydraulics etc.). Mechanical noise can be scattered directly from the source to the air, or follow a path in the structure and radiate from other surfaces acting as loudspeakers. This kind of noise is a minor concern since its energy level is relatively low and many design features like flexible couplings, splitted nacelle casing and acoustic insulators can drastically reduce the noise emitted. *Aerodynamically* generated (flow-induced) noise is instead capable of much higher sound power radiation, and many complex flow phenomena are at its origin. The better known ones, which regard particularly the wind turbines, are:

- Low-frequency noise, not tonal but related to a specific frequency (BPF, blade passing frequency). This noise is related to the interaction of a blade with the inflow altered by wakes shed by other blades, or by other obstacles. This generates local inflow deficiencies and an unsteady loading of the blade. This kind of noise is related to the construction of the turbine and its positioning, and can be reduced with a proper wind turbine designing.

- Interaction of blades with atmospheric turbulence, contributing to broadband noise in a not yet well quantified way. However, a distinction can be made between eddies composing the incoming turbulence, when their size is comparable with the airfoil chord c. If their diameter is comparable with the length c, its treatment can be analysed easily and is of M^6 dependence. If their size is much smaller than c, they are expected to interact with the surface (particularly complex is the interaction at trailing and leading edge) originating surface pressure variations that do not affect the global aerodynamic force, but will only cause local variations that can originate noise emissions up to 1000Hz with a M^5 dependency. Their analysis is therefore not yet fully understood.

- Trailing edge noise: originated by the interaction of boundary layer with blade trailing edge. The eddies contained in the boundary layer induce a fluctuating pressure field on the outer fluid field, but this interaction is not an efficient sound source. When the eddies come to the trailing edge, which is a sharp surface, they become source of relevant noise emission, contributing with a high frequency broadband noise which is perceived as a swishing noise. It is determined by the eddy convection speed and by the characteristics the boundary layer possesses near to the trailing edge, and mainly the distribution of turbulent kinetic energy normal to the surface.

- Interaction of turbulence at separation points, when present, generating broadband noise. This is the major contributing noise when the blade is stalled and can be prevented by avoiding the stall conditions, by means of a different turbine control system, a proper airfoil design and/or by using AFC to control the boundary layer;

- Blunt trailing edge noise, tonal type noise originated by vortex shedding mechanism, it can be avoided by correctly shaping and sharpening the trailing edge as much as it stays practical for production, handling and maintenance. The typical thickness for wind turbine blades is about 1–3mm;

- Laminar boundary layer noise is a tonal type noise and is originated from portions of laminar flow when it reaches particular instability conditions. It can also interact with the trailing edge

and lead to high levels of noise. This noise source is a negligible contributions since nowadays the high Re numbers at which the wind turbines operate ($\mathrm{Re} > 3 \cdot 10^6$) restrict the laminar flow zone to a small portion of the initial chord length;

- Blade tip noise, originated by the interaction of tip vortexes with the side edges of the blade. This noise is of broad-band character, and the strategies proposed so far to reduce it are to employ specifically designed tip shapes.

- Other noise originated by surface imperfections. The real operating blade can be subjected to many circumstances giving rise to flow disturbance and thus, additional noise. For example, the presence of surface damages due to impacts, lightning strikes, dirt due to insects and dust, presence of slits, holes and too loose production tolerances. All of them are potential origins of shear flows and vortex shedding, and some of them can never be eliminated but only mitigated by appropriate designing and correct maintenance.

The subject of this thesis is exactly the trailing edge noise, having the meaning just exposed. Its origin, bound to the interaction between turbulent eddies in the boundary layer and the sharp trailing edge, explain the origin of the acronym TBL-TE noise. In addition, an innovative idea to control and reduce noise emission is to alter directly the boundary layer structure and the wall pressure fluctuations that it originates, and consequently the noise scattering at the trailing edge. In the past decades, a huge effort has been made in attempt to bring the aerodynamic applications (especially airplanes, in the post second world war period) to a whole next level. After all the possible improvements were made by designing efficient structures, and manufacturing smoother and more regular surfaces, the successive step was deemed to be the artificial controlling of the boundary layer over airfoils, in order to reduce drag effects to previously unreachable low levels. These findings from the past works of many authors will be discussed when introducing ANC in Section 4.

1.3 Objectives

The goal of the present thesis is to validate the noise prediction tool Rnoise in development at IAG, in order to confirm it as a reliable foundation and proceed to airfoil optimization and Active Noise Control investigations. This is mandatory to make sure that predicted improvements will actually take place once they are concretised on real wind turbines. To achieve this, the specific objectives here to pursue are:

- Collect a sufficient number of real experiments conducted in wind tunnel facilities from literature. The availability of these is not so extensive, since it has to be ensured to have at least results for far-field noise measurements and that the operating conditions are mostly known, and do not constitute fundamental incongruities with a CFD bidimensional simulation of the same cases.

- Analyse these cases via CFD simulations using FLOWer software and subsequently Rnoise tool.

- Analyse and comment the results and gain new informations, i.e. which are the possible problems related to Rnoise and if it presents bad previsions with some specific airfoil shapes.

- Examine, like similarly done in the previous point, CFD simulations of ANC on a NACA64-418 airfoil realized through boundary layer suction. Determine which possible new methodologies of ANC are trusted to be useful and are likely to be concretised in future experiments.

- Gather a final conclusion to help future wind turbine noise TBL-TE studies.

2 TBL-TE Noise

This chapter is dedicated to the description of the turbulent boundary-layer trailing-edge interaction (TBL-TE) noise. This kind of noise is generated by turbulent flows which develop in the vicinity of a solid boundary and interacts with a sharp trailing-edge. To clearly explain the mechanics of a turbulent BL, an introductory explanation of the main aspects of a turbulent BL is handed.
An overview of the description and prediction methods available today is gathered, with a brief explanation of the theoretical principles behind the study of aeroacoustics.

2.1 What is TBL-TE noise

The turbulent boundary-layer trailing-edge interaction (TBL-TE) assumes firstly the existence of a turbulent type BL attached to the surface of a body. The eddies developed in the BL originate fluctuating pressures at the wall (WPF) that are indeed a very complex phenomenon, difficult even to observe and measure, thus also to model and predict. These fluctuating pressures can be induced by eddies of various sizes and are not efficient sound sources by themselves. Nevertheless, when they flow to the sharp trailing edge, they interact with it and become efficient sound sources and they can propagate waves of pressure which extends over a wide range of frequencies. This means that this kind of noise is not a tonal-type noise, but a broad-band phenomena which usually encloses frequencies between 200–8000Hz (the effective range may be narrower, this depends on flow conditions and airfoil shape). The conditions of non separated flow, turbulent boundary layer and sharp trailing edge are necessary to remain in the field of TBL-TE noise. The lack of any of these conditions, or the presence of other contributions (e.g. turbulence in the incoming flow, blunt TE) regards situations that are extraneous to the TBL-TE problem.

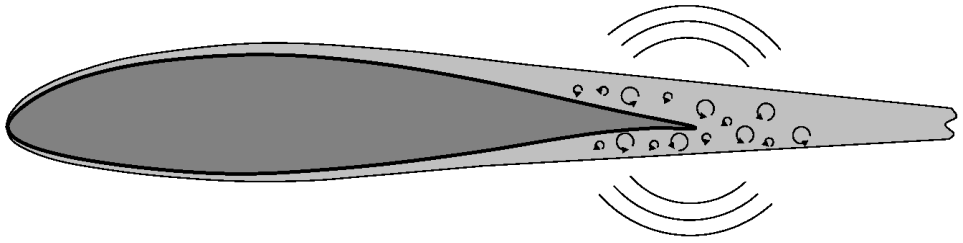

Figure 2.1: Mechanism of TBL-TE.

2.1.1 Turbulence description

Turbulence is in fact the most complicated form of fluid motion, but the most occurring in practical applications. This explains the need to model a turbulent flow since it is very important for its interaction with the surroundings and the equilibrium of forces. On most practical applications, the Reynolds number of a flow around an airfoil is high enough, that transition will occur at a certain point, turning the initial boundary layer from laminar to turbulent. Because of the geometry of the airfoil, the flow out of the BL gives rise to a pressure distribution on the outer edge of the boundary layer. This pressure distribution can be seen as imposed onto the outer surface of the BL, meaning that it is reasonably right to assume that pressure gradients perpendicular to the wall do not take place, then they are instead only a function of x. This is justified with the fact that the BLs are very thin compared to the airfoil radius of curvature, thus the only causes of pressure gradients in directions perpendicular to the wall (compensation for centrifugal forces) belong to a much larger scale [40, Chap.2].
As the boundary layer develops in this sense, the BL thickness δ will increase and the wall shear stress will decrease. The pressure distribution in the x direction is then of main importance in the formation of the BL and in fact determines strongly the position of the laminar-turbulent transition [40, p. 35–38], as long as transition is not artificially induced through application of grit, tapes, etc. The assumed expression which defines the *viscous shear stress* in the direction of x (frictional force per unit area), for a laminar flow, the *Newton's law of friction* [40, p.5]

$$\tau = \mu \frac{\partial U_1}{\partial y_2} \tag{2.1}$$

is no longer valid. The phenomenon of turbulent transition happens in a finite length space that is however considerable as a sudden happening. At the transition point the layer thickness increases suddenly, and so does the quantity of shear stress at the wall position. To describe the TBL, to the viscous shear stress previously defined as in Newton's law of friction an additional shear stress called *Reynolds stress* is included. The total shear stress in the x direction is then the sum of the viscous stress and the Reynolds stress [40, p.562]

$$\tau = \mu \frac{\partial U_1}{\partial y_2} - \rho \langle u_1 u_2 \rangle \tag{2.2}$$

A intuitive explanation of this addiction (and the influence of velocity u_2 on the stress acting on x) is given: being that the particles of fluid subjected to turbulent motion, while oscillating around a mean value (eddying motion), they do transport a momentum flux in every direction. This flux of momentum is equivalent to a force per unit area (a stress) which accelerates continuously the particles back and forth from zones with different velocity, thus altering their velocities. Among the overall consequences of this, one is also that the mean motion of the flow is affected, originating a behaviour similar to that of a fluid with increased viscosity, effect that is only apparent. At the wall, where $u_1 = u_2 = 0$ the Reynolds stress is zero and the viscous shear stress gets its wall-stress value τ_w. It is useful to define some other parameters to show how τ evolves in a turbulent boundary layer. Employing the kinematic viscosity ν which is an important scaling parameter in the near wall region, it is possible to define a *friction velocity* u_τ and a viscous length scale δ_ν by

$$u_\tau \equiv \sqrt{\frac{\tau_w}{\rho}} \tag{2.3}$$

$$\delta_\nu \equiv \frac{\nu}{u_\tau} = \nu\sqrt{\frac{\rho}{\tau_w}} \tag{2.4}$$

From these we derive a non-dimensional velocity and a *viscous length* in wall units

$$u^+ \equiv \frac{U_1}{u_\tau} \tag{2.5}$$

$$y^+ \equiv \frac{y_2}{\delta_\nu} = \frac{u_\tau}{y_2\nu} \tag{2.6}$$

This viscous length is useful to distinguish the different regions in the BL where the velocity distribution is determined by different mechanisms (Fig. 2.2). In the most closer distance ($0 < y^+ < 5$) a *viscous sublayer* is defined, a peculiarity of turbulent BLs. Its definition is necessary, since a turbulent BL is not longer just dominated by friction forces, like a laminar BL. It is still subjected to dissipation (thus also called *frictional layer*), but the direct effect of molecular viscosity on the shear stress exists only in a portion of it. In a viscous sublayer the inertial effects are negligible and the origin of shear stress is mainly from viscous effects. The successive region is distinguished when Reynolds stresses gain importance, but viscous effects are still a significant contribution. Its limit, found to be around $y^+ = 50$, encloses the region called *viscous wall region* and marks the beginning of the *outer layer*. The *log-layer* is the region where the shear stress is almost constant, and dominated by the Reynolds stresses contribution. Here the inertia terms are still negligible but the turbulent shear stress dominates the viscous shear stress. In this layer the velocity is correctly described by the *log-law*, and its limits of validity are between $y^+ = 30$ and $\frac{y}{\delta} < 0,3$. A mixing layer extending between viscous sublayer and log layer is called *buffer layer*.
Finally, the *defect layer* extends between the log layer and the edge of the boundary layer. In this outer layer, the velocity distribution deviates from the log-law [35, Chap.7]. In conclusion, the turbulent BL has a multi-layered structure and the larger portion is only apparently frictional, giving rise to dissipations which are but due to the turbulent fluctuating motion, and only a thinner, truly, frictional layer.

2.1.2 Mean velocity profiles

A fully developed turbulent BL is completely described by the quantities $U_1, y_2, \rho, \nu, \delta$ and u_τ, and dimensional analysis suggests the existence of a functional relationship between 3 dimensionless groups. The most famous, empirically determined relationship for turbulent BL is called *law of the wall* and describes the wall normal mean velocity distribution, and extends its validity in the buffer layer too, but not into the defect layer. Coles [6] showed that, instead, to describe the whole BL in an equilibrium condition, the mean velocity profile is well represented by the sum of two functions, one is the law of the wall and the second is called *law of the wake* and their only parameters are y^+

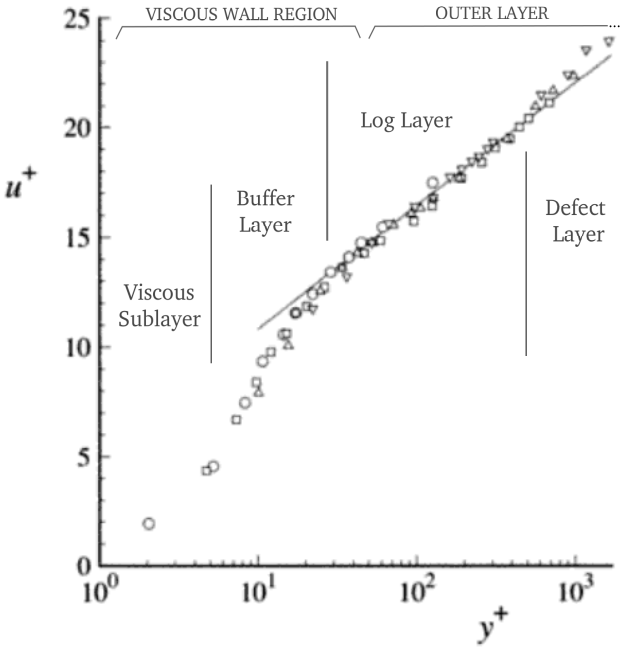

Figure 2.2: Mean velocity profiles in a turbulent channel flow and wall regions and layers after Pope [35]. Symbols: data from Wei and Willmarth (1989). Line: log-law.

and y_2/δ respectively. Namely, the equation involved is called *composite law of the wall, law of the wake* [6]

$$\frac{U_1}{u_\tau} = \left[\frac{1}{k} ln(y^+) + B + \frac{\Pi_k}{k} sin^2\left(\frac{\pi}{2}\frac{y_2}{\delta}\right)\right] \tag{2.7}$$

The *wake function* is the name of the third right hand term, and is assumed to be universal and has been originally tabulated by Coles. The non-dimensional quantity Π_k is the *Cole's wake strength parameter*, and is flow dependent (i.e. from the pressure gradient acting on the BL). k is the Von Kármán constant and B the law of the wall constant. Π_k can be estimated using the relation

$$\Pi_k = 0.6 + 0,51\beta_T - 0,01{\beta_T}^2 \tag{2.8}$$

where

$$\beta_T = \frac{\delta^*}{\tau_w}\frac{dP}{dx} \tag{2.9}$$

As may be deduced, the value of Π_k in the basic case of the flat plate is 0,6.

2.2 State of the art

In attempt to design low noise airfoils, the theoretical prediction of generated noise is the key means to fulfil an efficient and quick design process. Unfortunately, the flows that generate the noise are usually non-linear, unsteady and turbulent. Typically the unsteady flow region contains significant vortical, eddying motions that develop on a much smaller scale than, say, the typical scale useful for aerodynamic considerations c. In a flow it is not possible to unambiguously separate the *flow* from

the *sound*. However, when the flow Mach number is small it is advantageous to separate the task of solving the flow, from that of noise prediction. Nevertheless developing a numerical method for noise approximation is a long and delicate task.

2.2.1 Empirical and semi-empirical methods

The governing equations are still the same valid for fluid dynamics application (Navier-Stokes equations), and the problem has been approached in the past decades with different strategies, starting from the Lighthill acoustic analogy [28]. Lighthill's acoustic analogy is a fundamental theory, which allows to compute the sound field radiated by a fluctuating portion of an unbounded flow region, by solving an analogous problem of forced oscillation. It is possible to classify these models by their complexity, since they evolved obviously starting from with the most simplified ones which met the scarcer computation resources available in the past years. One well known model of this type is the Brooks, Pope and Marcolini (BPM) [5] method, based on experimental airfoil self-noise data sets. A major limit for it is that it does not take into account the airfoil shape and the flow regime. This model and the similar ones, classified as *Empirical or Semi-Empirical Methods*, have been used for airfoil low noise design but, due to these kind of limitations, are not suitable for a demanding optimization process. Other methods that fall in this category are Corcos [8], Chase [10], Howe [19], Blake [4], limited by assumption of zero pressure gradient, two-dimensional, turbulent boundary layers. Basing on Chase's work, Goody [13] developed afterwards a better model which incorporates the effect of Reynolds number by using only a function of the ratio of time scales of the outer and inner boundary layer, but is still limited to bi-dimensional, zero-pressure-gradient BL. Based on the empirical Goody model spectrum, very recently Rozenberg el al. [39], proposed an improved empirical surface spectrum model taking into account the effect of the adverse pressure gradient, and focusing on fan blades.

2.2.2 Computational Aeroacoustics (CAA)

In the recent years, the improvement of calculation resources has cleared the way for directly simulating acoustic scattering from trailing edges or lifting surfaces. The most popular, efficient methodologies of CAA in terms of computational costs are the *hybrid* methods. This means that the computation starts at the very beginning by solving unsteady Navier-Stokes equations together with a range of turbulence-handling techniques, and input this solution to successive sound propagation and radiation calculations over a larger scale. Unsteady RANS solvers are used to calculate the sources, and the acoustic analogies (Lighthill, Ffowcs-Williams-Hawkings (FW-H) analogies) to "translate" them in wave propagations. Also, the standard models for aeroacoustics are all based on the linearised Euler equations (LEE). These neglect the influence of friction effects for the propagation of perturbations. Based on this, further model assumptions lead to a variety of different available models, like Acoustic Perturbation Equations (APE).
Another class of low computational cost recently developed hybrid CAA methods is called RANS-CAA +. It is a stochastic turbulence generation based method, and uses steady RANS results to reconstruct the time dependent noise source or near-field by a stochastic algorithm. The main advantage is that it's being able to predict broadband sound at much lower computational cost compared to unsteady RANS based CAA simulations. However, the RANS-CAA + methods suffer from inaccu-

racy in the generated sound prediction, due to a possibly inaccurate reconstruction of the turbulent velocity field properties. The CAA methods are nowadays still not enough advanced for them to be generally applied for practical design work. They have at most the function of observation and understanding sound propagation phenomena.
A comprehensive survey about CAA methods can be found in [7], and an useful source at [2].

2.2.3 Simplified theoretical models

These models rely on the spectral solution of a Poisson equation to obtain a representation of WPFs underneath a TBL, and calculate the propagation of noise emission from the trailing-edge due to this fluctuating pressure by solving a diffraction problem. However, to relate velocity field and WPFs is not an easy task.
Kraichnan [26], Amiet [1], were the first to attempt this, by reporting theoretical estimates of the mean square wall pressure and spectra based on the Poisson equation. In Amiet's method, the trailing-edge noise is derived by iteratively solving scattering problems at the airfoil edges. The main trailing-edge scattering is first determined by assuming that the airfoil surface extends toward infinity in the upstream direction. Amiet reduced the formulation to this first evaluation and calculated the radiated sound field by integrating the induced surface sources on the actual chord length c and the span length L. This provides a first evaluation of the radiation integral. A leading edge correction, fully taking into account the finite chord length has been derived by Roger and Moreau [38].
Finally, after the previously mentioned Blake model [4], which is a wavenumber-frequency spectrum model (and still an empirical relationship having the mentioned disadvantages), Parchen [33] successively developed a trailing-edge noise prediction model known as *TNO-Blake model*. This last result is at the basis of Rnoise code, chosen because a routinely designed, fast, less expensive and accurate prediction method is desired. A simplified theoretical model like this is thought to be in one hand accurate and efficient, and on the other hand takes the very specific airfoil BL characteristics into account.

2.3 Overview of Rnoise code and related theory

As previously stated, the noise prediction method utilized in the present work follows Parchen [33] model. Essentially, it solves the Poisson equation for the spectrum of surface pressure fluctuations, and evaluates the noise emission from the trailing edge due to this fluctuating pressure by solving a diffraction problem -that is, the fluid oscillations that propagate from a semi-infinite edge trough an acoustic medium that is treated as incompressible-. On a first step, the spectrum of the wall surface fluctuations is obtained as follows [33, Eqn. 2.20]

$$P(k_1,k_3,\omega) = 4\rho^2\left(\frac{k_1^2}{k_1^2+k_3^2}\right)\int_0^\infty\left[\frac{dU_1(y_2)}{dy_2}\right]^2\cdot\Lambda_2(y_2)\cdot\tilde{\phi}_{22}(k_1,k_3),$$
$$\cdot\langle u_2^2\rangle\cdot\phi_m(\omega-k_1U_c)\cdot e^{-2|\mathbf{k}|y_2}dy_2 \tag{2.10}$$

Φ_m is the *moving axis spectrum* and needs to be modelled with care. It carries the meaning of

describing how the generation and destruction of the eddies during their convection past the trailing-edge distorts the spectrum of the fluctuations. In its original formulation by TNO is function of other BL quantities and contains an empirical constant. The integral scale Λ_2 is the integral length scale in wall normal direction, thus referred to the vertical velocity component. It is defined as the integral of $\tilde{R}_{22}$ (the normalized spatial two-point correlation coefficient of the vertical velocity fluctuations u_2) in the y direction, from the wall to infinity (but practically in this case, until the boundary layer thickness is reached).

$$\Lambda_2 = \int_0^\infty \tilde{R}_{22}(r_2)dr_2 = \int_0^\infty \frac{\langle u_2(y_2,t) \cdot u_2(y_2+r_2,t)\rangle}{\sqrt{\langle u_2^2(y_2,t)\rangle} \cdot \sqrt{\langle u_2^2(y_2+r_2,t)\rangle}} dr_2 \tag{2.11}$$

Once the spectrum of the WPFs is known, the noise scattered from the TE is calculated by representing the WPFs as a distribution of harmonic waves. According to [33, Eqn.2.23],

$$S_{ff}(\omega) = \frac{1}{4\pi R^2}\frac{\omega L}{c_0}\int_{-\infty}^{\infty} \frac{P(k_1,0,\omega)}{\mid k_1 \mid} dk_1 \tag{2.12}$$

All the necessary input turbulence noise parameters (from here on, "parameters") $\langle u_2^2\rangle$, $\frac{dU_1}{dy_2}$, Λ_2, $\tilde{\phi}_{22}$ and ϕ_m in these equations are related to the structure of the BL in proximity of the airfoil TE. Different prediction codes have been developed, following the work of Parchen et al. to derive these parameters: NAFNoise [30](developed by NREL, USA), RISØ-XFOIL [3] (developed by RISØ-DTU, Denmark), and Xnoise [18] (developed by IAG of University of Stuttgart). All the cited tools employ the XFOIL software [11] for the parameters derivation, using relations valid for zero pressure gradient (flat plate) isotropic TBL.
Note that for the parameters required from Eqn.2.3, RANS calculations yield only $\langle u_2^2\rangle$ and $\frac{dU_1}{dy_2}$, while $\langle u_2^2\rangle$ can be available if a full RMS turbulence model is used, or derived from k_T in the case of the SST model. All the other terms need to be modelled, and the accuracy of the results will be very sensitive to how accurately these parameters are modelled. There is no unique way to obtain them, for example they can be determined from elaborate finite-difference BL calculations, or directly from measurements. Rnoise is conceived to read the RANS based solver DLR FLOWer (Sec.3.1) results, and compute the parameters related to the TNO-Blake model applying an *anisotropy scaling method* [22, Sec.3.4.3], thus allowing a more elaborate parameter derivation, also basing itself on different turbulence models (i.e, all the turbulence models supported by FLOWer, described in Sec.3.1). For the purpose, many different modelling approaches are selectable within Rnoise (the isotropic approach too) and will be referred from this point on with the prefix "mp", and their meaning is explained in Sec.3.4. For a more extensive explanation on how Rnoise derives these parameters, see [22].

2.4 Noise reduction by means of Active Flow Control

As pointed out in Sec.1.1, active control on the turbulent boundary layer is trusted to be an effective means for noise reduction. The noise reduction is realized by suction of a small amount of the boundary layer into the airfoil, thus not by turning the flow back to the laminar flow regime. The

experiments conducted by Wolf et al.[44] confirmed this experimentally and the predictions calculated using Rnoise showed good agreement. The experiments were aimed to get a first confirmation of the expected results, and some different configurations for the actuator were tested, both varying actuation location and intensity in terms of the non-dimensional *suction coefficient* C_Q (see Eqn.4.1). Conclusions based on the experimental results were derived in relation to the variation of these parameters. It would be useful, if one could individuate which are the best position and suction coefficient in terms of the altered SPL, c_l and c_d, but it is clearly extremely complicated since a possible optimum point may be a function of many parameters like Re, actuator surface, airfoil shape and many more. Thus, the factors which determine an optimal condition for the actuator and how they influence the results, may only be deducted by observing more experimental cases.
The principal information deducted by the experiments of Wolf et al. are:

- With suction, the velocity profile in the very proximity of the actuator becomes fuller and the boundary layer thickness is reduced. The fluctuations are reduced except in the region very close to the surface, where an increase can be recognized.

- The configuration where the actuators were positioned from 55% to 65% of chord shows better results than the one with the actuator positioned from 65% to 75% of chord. In this case, however, the associated fluctuations in the centre of the near wake are stronger.

- A significant noise reduction is achieved at the lower frequencies (frequencies lower than 2000Hz), which dominate the overall noise level. The peak amplitude decreases and is shifted to higher frequencies. At high frequencies the noise emission slightly increases, due to the stronger velocity fluctuations close to the airfoil surface, associated with smaller eddies that reside close to the surface. A higher suction rate strengthens these effects.

- After a preliminary, optimistic evaluation of the drag generated by the loss of momentum in the sucked mass flow, the results indicate that there is still an overall reduction of total drag, but only for the higher AoA of 6°.

- The experiments revealed that the noise can be reduced by up to 5dB with 6°AoA with the employed resources. Concomitantly lift increases and drag reduces. This effect is deteriorated for smaller AoA, which for a 0°value gives smaller maximum noise reduction (4dB) and higher c_d than the baseline case.

- The effective pump power needed has to be evaluated and contains a lot of unknown factors. Some of them are the pressure loss due to the transit trough the porous plate and the pipes, the efficiency of the pump and the difference of pressure respect to the airfoil surface pressure, which is clearly not constant even along the actuator length itself.

At this point it may be also useful to mention the past researches done on the argument, which are part of the major field of study known as Boundary Layer Control (BLC). Renowned works like those from Schlichting [40] and Lachmann [15] demonstrate how broad and settled was already the knowledge about BLC, and how was already clear that the step further in the improvements of aerodynamic performances has to deal with the control of the boundary layer. In detail, Schlichting [40, p. 383-399] demonstrated already results of boundary layer suction, showing its effectiveness in either obtaining more lift or more lift/drag ratio, by *retarding the turbulent transition* or *preventing separation*. This is properly explained by observing that the effect of suction is to remove the lowest-energy particles, which are the origin of these phenomenons. The boundary layer thickness is then

reduced and its velocity profile can be even altered to a prescribed shape, and a "new" boundary layer is allowed to grow and to bring the expected advantages. In the majority of the cases this does not mean to remove the entire BL, but only the lowest energy layers close to the surface profile instead. Lachmann [15] also presents a very notable gathering of methods aimed to boundary layer control and shows its effectiveness with many experimental measurements, with the same intent of reducing drag and retard or even totally prevent turbulent transition. This is not of interest since the flow over a wind turbine blade is expected to be mostly turbulent, due to unavoidable surface roughening, unstable inflow conditions and a generally high inflow Reynolds number. Nevertheless, this idea is at the basis of this noise control technique, since the boundary layer thickness and its content is likewise responsible of TBL-TE noise scattering. Schlichting [40, chap. 17] also expands the problem by considering which are the optimal engineering solutions considering the power needed from a pump to actually concretise the suction, which is problem of no minor importance.
This is also an aspect to consider in the present work, therefore an eye on which are the best actuation conditions and their effective advantages will be kept.

The mentioned sources of Lachmann and Schlichting reports an abundant quantity of studies and experiments, along with a critical evaluation. The main objective of these efforts were to find good solutions employing air suction, blowing or both of them to gain a reduction in drag, improved lift and stall behaviour of profiles and wings. An eye is always kept on the feasibility and the engineering problems related to these solutions. It happens that almost all these experiments are dealing with laminar boundary layer and/or the application of control surface like ailerons, flaps and slats, or the study of flat plates, all of these applications are extraneous to the application of turbulent BL on wind turbine profiles. Nevertheless, these results may be useful to understand the principles at the origin of this form of BLC which may apply to ANC over an airfoil.
Lachmann (p. 204) reports an example of calculations of the minimum suction C_Q needed to prevent separation of a TBL, and resulted that the best solution is to concentrate the suction on the forward part (<0.2c) of the airfoil. More extended length of actuator surface required more suction mass flow to achieve the same result. This may indicate that the air which is mostly subjected to energy loss at the leading edge, is responsible of separation when it encounters the adverse pressure gradient, like observed in the simple cylinder example of Schlichting [40, Chap.2]. The concentration of mass removal on the leading edge may mean to remove air from this early formed boundary layer as much as possible.
Lachmann (p. 964) reports also an experiment of suction in a laminar tube. In spite this experiment is also not very representative of the current problem (in the tube the flow slows down due to the suction), it is interesting to see that in conclusion the best solution which attains less pressure loss across the suction device is a large number of spanwise slots cut in a very thin skin bonded on a thicker skin, the latter having the effective suction holes drilled. It is also worth to note the realization of individual suction pressure for each group of ten slots, by means of needle valves. Different suction chambers, each with a different suction pressure may be needed if the actuator length is usually longer than 5% of the chord, due to the non constant pressure along the airfoil. Figure 2.3 shows how actuating a constant pressure condition on the suction side, means that the required pressure to attain the desired massflow originates a rising difference of pressure in the direction of flow, hence an increasing suction velocity. If the actuator is too long in relation to the steepness of c_p, it may turn out that in the more upstream part of the actuator, no pressure difference or even reversed pressure difference establish, the latter causing the blowing of air, and leading to an unpractical and/or non-physical situation.

The subsequent experiment reported in the text by Lachmann also demonstrates the feasibility of suction applied on a wing plane (F-94) at high Re, by applying distributed suction on a wing section

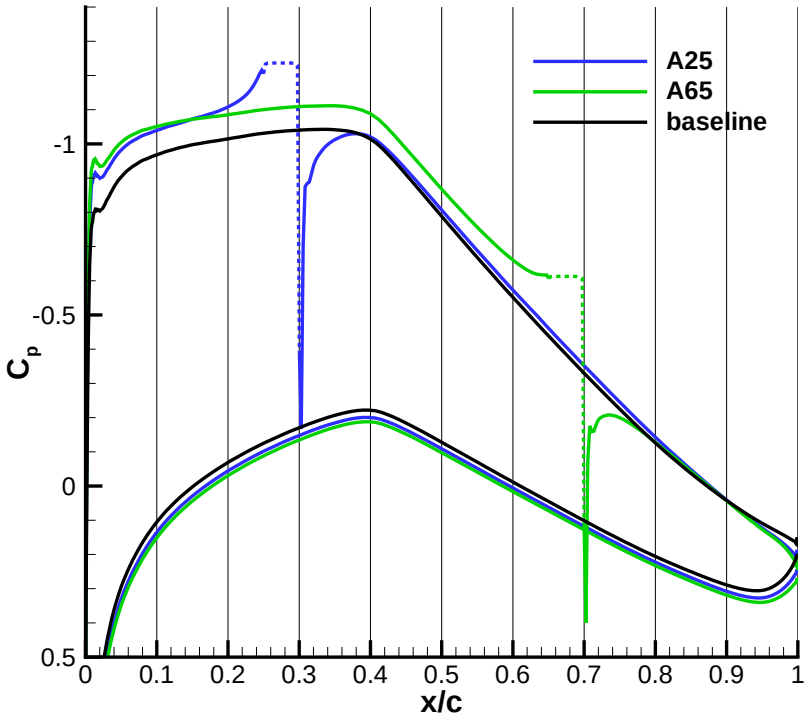

Figure 2.3: Typical effect of a single actuator on the C_p of a NACA64-418 airfoil at Re $2,5 \cdot 10^6$, 6°AoA and Mach 0,206. The actuator positions of 0.25c (A25) and 0.65c (A65) are shown. The dotted portions refer to the real actuator surfaces.

to obtain full chord laminar flow. Aside from all the observations, it stands out that while increasing suction, a point of minimum drag is obtained, further suction causes the BL to get thinner and thus causing more friction, obtaining an overall increase of drag. The drag also increases when Re is reduced and the optimal suction rate is maintained, since this optimum suction rate is higher, causing higher C_L and higher speeds on the suction side. Schlichting reports also a solution and experimental validation of suction on a flat plate. It is moreover an exact solution of the Navier-Stokes equation, but it is not fitting with the investigated conditions (there is no zero-pressure gradient and no imposed vertical suction velocity v_s). It is however useful to understand some phenomenons like suction drag and that the BL still grows even along the suction surface.
All these observations suggest that the causes of noise are different from those pointed out in the literature at the basis of skin friction drag and turbulence transition. The improvements sought in the cited literature are different indeed from those of noise reduction, thus it was expected that the same mechanisms that alleviate drag and turbulent transition were also linked to noise reduction. The results obtained (see Sec. 4.3) indicate that the optimal parameters for noise reduction behave differently when aimed to the noise reduction, than in the case of search for minimum drag and delayed turbulent transition.
In the present days, the research for applications of AFC is not oriented towards noise reduction as much as like towards aerodynamic performances. In this direction the work of Guo [14] can be cited. The author worked on a sophisticated actuator system, by employing pulsating jets deployed on a

wing span model and considered the possible noise emissions. A major concern in this case is to avoid an even louder noise caused by the actuator system itself. More applied experiments in this period like those from Kosin [25] report applications of suction conceived as part of an airplane's design, turning it into a "Laminar flow control airplane" capable of extending its range or payload by one third. This is stated by showing that is possible, by applying a small amount of continuous suction along the leading edge and the suction side of a swept wing, to maintain laminar flow at very high Reynolds numbers. Actually many efforts are made in the field of AFC to improve the whole knowledge and performance of vehicles [42], and BLC is only one between many other research topics. Gad-el-Hak and Blackwelder [12] investigated a way to block transition by controlled suction applied only when needed, namely, in case of ejection of low-speed streaks from the wall region. Kerho [29] developed a way to detect these low-speed streaks and proposes a different way of applying suction to reduce drag, by developing a system of sensor, control and actuators capable of intermittent suction, realizing very low suction coefficients C_Q, demonstrating this option as being a more feasible concept from an energy balance standpoint. A reference to compare qualitatively the results obtained in this work, is from Antonia et al.[36], which presents the effects of concentrated suction and sudden change in the boundary layer conditions. He observed with particular attention the effect on Reynolds stresses and how quickly they "recover" after the sudden change imposed by the actuator. Unfortunately, relaminarization of the BL is investigated, and this is not the aim of the present work, making the results not comparable. Park [34] did a similar work with numerical DNS simulations, investigating the effect of suction on the mean and fluctuating velocities in all directions. Interesting result is that suction draws the near-wall streamwise vortices towards the wall, where viscous diffusion is more effective, resulting in weaker streamwise vortices in the *downstream* of the slot. Therefore, the turbulence intensities as well as the skin friction decreased only downstream of the slot.

3 Far Field Noise Prediction Validation

In this chapter the adopted methodologies of analysis are explained as clearly as possible, in order for the reader to understand the procedures behind the results in section 3.4. A summary of the test conditions of the various experiments considered is provided, followed by the discussion of the results.

3.1 Description of adopted analysis routine

A great advantage of using a tool like Rnoise is that the software can be fed with steady-state RANS simulation solutions, which are a standard, already well settled and known technique for aerodynamic design. They are also relatively quick to compute (compared to unsteady CFD and DNS). This allows to plan a fast analysis routine adopted in the present work, which is described in the followings. The complete (flowfield, boundary layer, and noise) analysis, takes only slightly more time than the time needed for the RANS simulations. This time, with the procedures to be exposed in the following and a modern dual-core 3GHz processor, lies around 12 hours.

FLOWer CFD solver The CFD software FLOWer solves the compressible RANS equations working on block structured grids. Being a density-based solver, it is optimized for the simulation of exterior flows in the compressible regime. FLOWer is developed by DLR with contributions from several German universities, and the present work makes use of a code modification which allows the modelling of steady actuators (blowing/suction) through a subroutine developed and tested at IAG [16]. This implementation has been configured in this analysis, to sub-iterate for every CFD iteration step, converging to the constant pressure along the actuator surface which realizes the desired massflow. The flow solver is parallelized based on MPI and is optimized for vector computers. For further informations on the solver structure, see reference [27].

Computational mesh and turbulence models Simulations were performed on C-type structured meshes counting of $672 \times 128 = 86016$ cells (Fig.3.1). The meshes are script generated, parametrized with Re and c, designed specifically to met boundary-layer resolution requirements. Namely, the y^+ values were assumed to be 1 at the first layer above the surface of the airfoil, providing more than 30 cells across the expected BL trough Reynolds number considerations. Computations were performed with two different turbulence models, and they will be marked in the subsequent results presentation. These are Menter's SST two-equation model and full Reynolds stress model (RSM). For the calculation of a consistent BL development, the point of expected transition is also provided to the solver. The adopted logic was to analyse then mostly tripped airfoil experiments, and utilize the XFOIL software [11] to predict the expected transition point in cases of natural transition. For

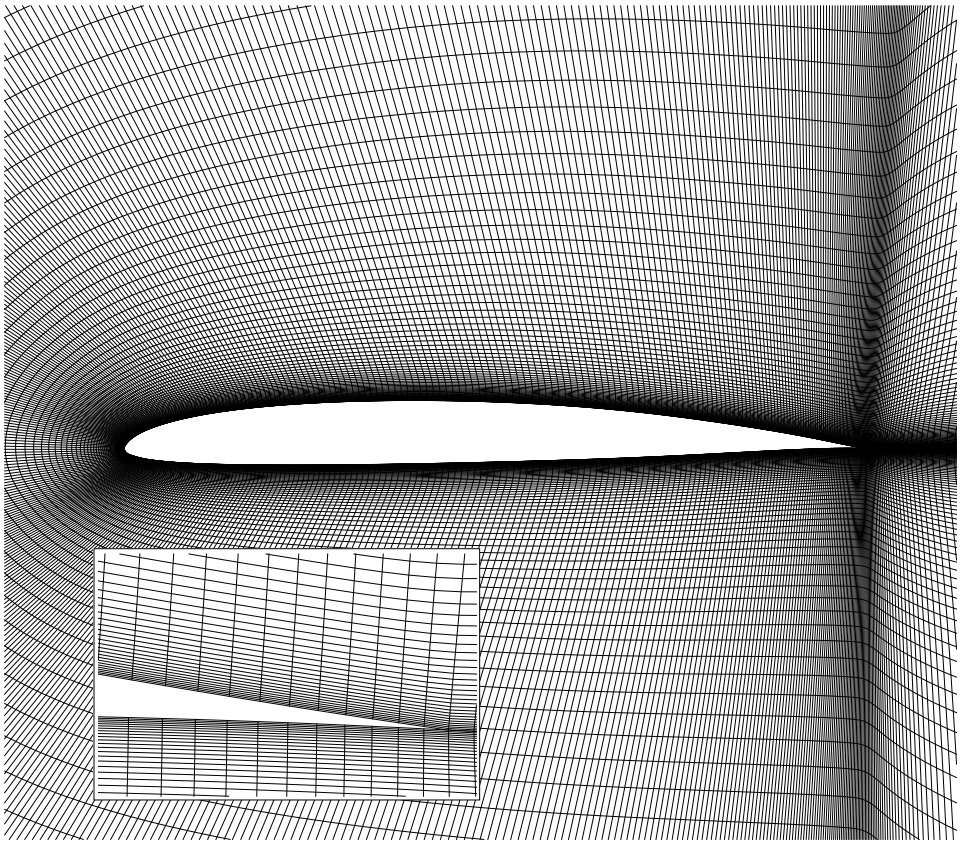

Figure 3.1: Example of the grid mesh employed for RANS calculations

the reasons discussed in Section 2.1, it is always preferable to investigate cases in which the BL is mostly turbulent, thus where the transition point is as close as possible to the LE. This also helps to give consistency to the analysis since the acoustic phenomenons to study are related to the fully developed turbulent BL. A laminar BL, instead, is source of different noise scattering mechanisms like laminar vortex shedding (Sec.1.1) which are not taken into account in the adopted model, described in Section 2.3.

Post processing The flow solver FLOWer provides an output file where all the flow variables are available in non dimensional form in a cell centred body fitted grid. In order to prepare the necessary turbulence parameters for the noise prediction model a previously developed post-processing tool has been extended in the Rnoise framework. This post-processing tool performs the appropriate coordinate transformations of the velocity vectors and the stress tensors of the computed flow solution, and finally re-dimensionalizes all flow variables. The enhanced tool also allows the evaluation of the integral boundary-layer parameters (IBLP) along the airfoil chord. The FLOWer solver results are then input in this post-processing tool which is part of Rnoise. This helps verification and investigation of the numerical and measured data in a user friendly way. It is to remark that within the analysis routine, the calculation time needed by Rnoise for analysing a single case lies around just some seconds.

3.2 Detail of the experimental data sources

Many results are available in literature in the field of aeroacoustic. Only a smaller part of them is specifically focused on TE acoustics problems, and a further smaller part of these offer complete, clear results suitable for the purposes of this thesis. The sources employed in this work are briefly exposed in the following paragraphs, among with their peculiarities, the latter necessary for a conscious observation of the results.

3.2.1 W. Devenport et al. [9]

This report provide a vast database of airfoil measurements, conducted at the Virginia Tech Stability Wind Tunnel, and sponsored by the National Renewable Energy Laboratory (NREL). Four airfoils were tested: DU96, S831 (developed at the NREL), NACA0012 and Risø B1-18. These last two have not been considered, since the NACA0012 has already been extensively studied and the B1-18 is a proprietary airfoil. This tunnel is a continuous, single-return, subsonic wind tunnel with 7.3m long removable rectangular test sections of square cross section. It features 7 turbulence-reducing screens and a 9:1 contraction nozzle for reducing turbulence levels. The facility is extensively described in [37].
Far-field noise were measured with an equal-aperture spiral microphone array, containing 63 electret microphones, and positioned behind a Kevlar acoustically transparent cloth outside the test section, at a distance of 3m, positioned over the airfoil rotation centre (at quarter of chord) and pointing towards it. The peculiarity of this sound measurement method is that being out of the air flow the instrument is incapacitated to contaminate it, but still does not suffer of jet-flow noise contamination like happens in open-jet wind tunnels. Data were collected in 12th-octave bands, thus they have been converted to 3rd-octave bands for comparison purposes. The authors warns about the fact that the surface which hosts the microphone array is acoustically reflective, thus higher values of SPL are read (6 dB higher than a previous brace-mounted array used in the same measurement campaign), but the frequency range affected by this addition is not known. Further, how this difference in the readings has to be accounted when comparing the results with measurements coming from other experiments is hard to guess, and will be considered in the observation of the results. It is expected that these results will have a certain amount of overestimation, of 6 dB maximum, respect to any other conventional measurement output. This microphone array is reported to have a measuring bandwidth of 500Hz to 5000Hz, and a SNR ratio of 15 at lower frequencies and 10 above 2000Hz.
With hot-wire anemometry, velocity profiles were measured in the vicinity of the trailing edge of the airfoils, on both PS and SS. The data were collected slightly downstream of the TE (maximum offset 2mm, that is approximately $0,2\%$ of chord length). This study therefore assumes that there was no significant evolution of the boundary-layer flow over this short distance.
The spectral data of the BL are also reported, but have been not used in the present work. Only the mean velocity fluctuation $\langle u_1^2 \rangle$ has been extracted for comparison. It is important to notice, that the S831 tripped experiments could not be included since they presented a certain amount of BL separation, thus the BL limit could not be defined at the TE and the related noise phenomenons were out of the adopted theory. Unfortunately these tripped experiments have been run only at relatively high AoA. A lower AoA should have been included in the experiments too, since the airfoil itself has a high maximum camber (see Tab. 5.1). This is anyway an unexpected outcome since it is commonly the BL with more developed turbulence the one less prone to separation. When possible, the experimental data related to BL and FF measurements which are in similar or almost identical

conditions have been gathered and compared. The Reynolds number and AoA will be always the same, only the inflow velocity appears to be different because it is an unknown data for the BL measurements, thus has been guessed along with the air density from the Reynolds number.
For all of them, the experimental values of SPL, U/U_e and $\langle u_1^2 \rangle$ are plotted along the corresponding results derived from the Rnoise calculations.

3.2.2 F. Hutcheson and T. Brooks [20]

This paper reports the trailing edge noise experiment performed at NASA Langley Research Center in the Quiet Flow Facility (QFF) in 2004. It is an open jet anechoic facility. In these measurements, a NACA63-215 airfoil is used and modified in a lot of different ways with grit, vortex generators or strips of serrated tape to trip the boundary layer. It is not clearly indicated on which cases which of these LE treatments are employed, thus this introduces inevitably an additional cause of dissimilarity with the simulations, making more caution needed when comparing them with CFD results. Many types of TE conformations are experimented, and since the only employable TE configuration for Rnoise and the related noise model is a sharp TE, only the configuration named #1 has been considered, being the sharpest one (namely the most similar to a sharp TE and measuring 0,6mm in thickness). The test conditions included mean flow Mach numbers ranging from 0,07 to 0,17 (corresponding to a chord Reynolds number ranging from about 0,6 to 1,6 millions). The airfoil was placed at angles of attack ranging from 6,2°to 8,8°, but corrections are applied due to the deflection of the incident flow caused by the finite size of the open jet. The effective angle variations spans then between -2,5°and 3,6°.
The measurements of the FF acoustics are made with a Small Aperture Directional Array (SADA), composed of 33 pressure microphones projecting from an acoustically treated frame. The SADA measurements are performed approximately five feet from the airfoil trailing edge, in the mid-span plane. The data from the 33 microphone channels were recorded simultaneously with the necessary treatment of low and high-pass filters, the final result Fourier transformed with a Hamming window treatment, obtaining a 17.45 Hz narrow-band frequency resolution which is then presented in one-third octave bands and scaled for a "per foot" presentation, namely for a 0,305m (1 foot) span airfoil observed from a 1,524m (5 foot) distance. The relevant results for the mentioned #1 configuration have been collected and compared with Rnoise results, giving a total of 4 entries in the test matrix (Tab.3.1).

3.2.3 S. Oerlemans [31]

Aeroacoustic measurements are available here for six airfoils, conducted at NREL's Small Anechoic Wind Tunnel KAT between 2002 and 2004. Tests were run for or a range of wind speeds and angles of attack, with and without boundary layer tripping. The tunnel is of the open loop type, open-jet discharged in a test section room covered with foam wedges. An effective angle of attack calculation has also been considered, which depended on the wind tunnel and chord length dimensions. The noise data have been gathered with a 48-microphone array of 0,8m $\times$ 0,6m for resolution considerations, placed outside the jet flow at a distance of 0,6m from tunnel axis, and centred with the tunnel's axis. Leading-edge and ps measurement were also conducted but here not utilized. In this particular test campaign is clearly shown how in the untripped condition many airfoils feature an intense tonal component of noise, which disappears with the application of tripping. Thus finally only for the

tripped cases of suction side, TE noise measurements have been here considered.
Unfortunately the test have been conducted at fairly low flow speeds and Re, this caused partial or total separation in the correspondent RANS simulations at some points of high cambered and/or high-AoA cases. It is not known if the same has happened in the experiments, but the higher irregularity and less agreement to the $U^{4,5}$ presented scaling rule may suggest so. These cases were also excluded from the analysis.
The authors also warn about the difficulties encountered with relatively low noise emissions from some cases at these low speeds, thus susceptible to background noise contamination. The author tried to individuate and exclude those points possibly contaminated by background and edge noises.

3.3 Test matrix

The test matrices which condenses the cases simulated with CFD is exposed in the following. Table 5.1 in the Appendix shows the main aerodynamic characteristics of the airfoils employed for experimental data validation.
Table 3.1 shows the experimental cases gathered, the origin of these data has been indexed in Sec.3.2. The turbulent transition position is intended as percent of chord length from LE at which the transition occours, for suction and pressure side respectively. In case a tripping device is not applied, the transition point is predicted using XFOIL software [11].

Airfoil	$Re \cdot 10^6$	M	α	c	U_∞	trans ss|ps %
DU96	1,69	0,084	3	0,914	29	48|70
	3,15	0,164	7	0,914	58	(5|10)
	3,15	0,166	7	0,914	59	35|74
S831	1,5	0,084	-2	0,914	29	69|53
NACA63-215	1,61	0,17	-2,5	0,406	58	64|48
	1,61	0,17	3,6	0,406	58	45|66
	1,04	0,11	-0,5	0,406	37	60|61
	1,04	0,11	3,6	0,406	37	49|69
S822	1	0,186	0	0,23	64	(2|5)
	1	0,186	4	0,23	64	(2|5)
S834	0,75	0,14	0	0,23	48	(2|5)
	0,75	0,14	4	0,23	48	(2|5)
SD2030	0,5	0,095	0	0,23	32	(2|5)
	0,5	0,095	4	0,23	32	(2|5)

Table 3.1: Test matrix of the gathered experimental data for comparison with noise prediction software. Transition point in brackets means the transition is forced with BL tripping.

3.4 Far-field and boundary layer results and analysis

In the following pictures the results of the comparison are shown, the different mode profiles for Rnoise are identified with the prefix "mp" and the mode mp6500 is reported in every picture. The digit 6 indicates that an anisotropic scaling function is employed, that characterizes the degree of anisotropy in the wall normal direction (or how far the flow is from the isotropic condition). In case of SST model, the velocity fluctuations $\langle u_i^2 \rangle$ are derived using this function and k_T. The value 4 for the first digit represents the use of anisotropic scaling function with extended Boussinesq hypothesis. This hypothesis is used in the development of most of the well known one/two-equation turbulence models. The advantage of this approach is the relatively low computational cost associated with the computation of the turbulent viscosity, the disadvantage is that it is able to model only weak anisotropy feature of the flow [23, p.59]. In the case the first digit is 1, instead, it is considered as proportional to k_T, without considering anisotropy of turbulence.
The second digit 5 means that Λ_{22} is a function of $\langle u_i^2 \rangle$ (in case of RSM) or k_T (in case of SST) as descripted in [22], and a *corrected* ϵ. Corrected ϵ means that the dissipation parameter is corrected with an empirical y^+-function which substantially alters it in the near-wall region of the viscous sublayer. This operation has been found to be needed and bringing positive effects [24, p.58] since the actual turbulence models cannot model the parameter in the viscous sublayer, due to the dissimilar mathematical description in the definition of ϵ between experimental and RANS approach. In the case the second digit is different from 5, this correction is not used.
The third digit distinguishes the use of two different description of the denoted moving axis spectrum Φ_m: the original TNO definition [22, Eqn.5.4] denoted by 0 and an improved model described in [22] is denoted by a 2.
The fourth digit indicates how the parameter U_c (which is contained in the original TNO definition of Φ_m) is modelled. U_c represents the velocity at which the pressure footprint, which eddies generates on the wall, moves along the wall. Large eddy structures in the mean will be found far away from the wall and hence move nearly with the free-stream velocity. Small eddy structures must be close to the wall to have a significant effect on the wall pressure and then, consequently, move slower if a usual boundary-layer profile is assumed. A 0 means U_c is treated as constant, proportional to U_∞. A 1 or 2 means it is given respectively by the more complex expressions cited in [21, Eqs.13,14].

The simulations on the DU96 airfoil can be compared also with the BL measurements available from the experiment authors. An important remark, is that the conditions between far-field noise measurements and BL hot-wire measurements was unfortunately not exactly the same. The cases here compared share always the same AoA and and the most similar flow condition. The effective flow conditions can be read in each plot (when different) and the noticeable differences in flow speed are only due to the fact that the speed is calculated from the given conditions, with the unknown of flow temperature which introduces an uncertainty when obtaining the flow speed from the given Re number. The first case shows a noise level agreement, and so does the extracted boundary layer profile near the TE and the Reynolds stress (Fig.3.2a).
The difference between turbulence models used is very little and the best fitting modes are mp6520 and mp4520. The agreement is good, even if it carries some uncertainties due to the unknown exact position of the transition point. The two successive cases at higher Reynolds number show worse agreement, and this is explainable with the different shape of the Reynolds stress calculated on the ss (Fig.3.2b) which overestimates the measurement in the distances closer to the wall, and underestimates it further from the wall. This is connected to an overestimation of high frequencies

and underestimation of low frequencies. The measurements done for Reynolds stress on the ps has suffered from a kind of inconvenient thus is not very well comparable. The SPL graph, which shows two different peaks (the leftmost peak is originated by the suction side TE noise) are also somewhat found in the measurements but their entity and peak frequency differs. The prediction of the ps side contribution resulted always more difficult.
Here there was the possibility to insert also data from a different experiment conducted at DLR AWB Braunschweig[17], which was conducted on slightly different flow conditions and thus an attempt to scale the results was made. The result is a curve which is not too different from the VT experiment, but fits much better with the prediction made. The agreement is worse for correspondent clean case (Fig.3.3a), in which the contribution of the ss looks very well predicted, but the one for the pressure side contribution is very different. Nevertheless, the uncommon shape of the ps Reynolds stress curve may be not an error, but due to another uncommon event which brings the ps pressure fluctuations out of the TBLE noise theory. Only the best fitting modes are shown, which produce either very similar results. Only the correlation length results different and much smaller when the SST model is employed, but the peak lies at the same wall distance of the RSM case. The noise overestimation found in both cases can be explained by the higher velocities calculated in the near wall distance.

As a general remark, the NREL profiles S831, S822 and S834 have always shown more difficulties in the simulation and comparison process, since their high camber and particular profile lead easily to recirculation zones in many of the simulations, in some cases making the prediction impossible, and the relatively low Reynolds numbers chosen do not help to alleviate the problem. The cases here

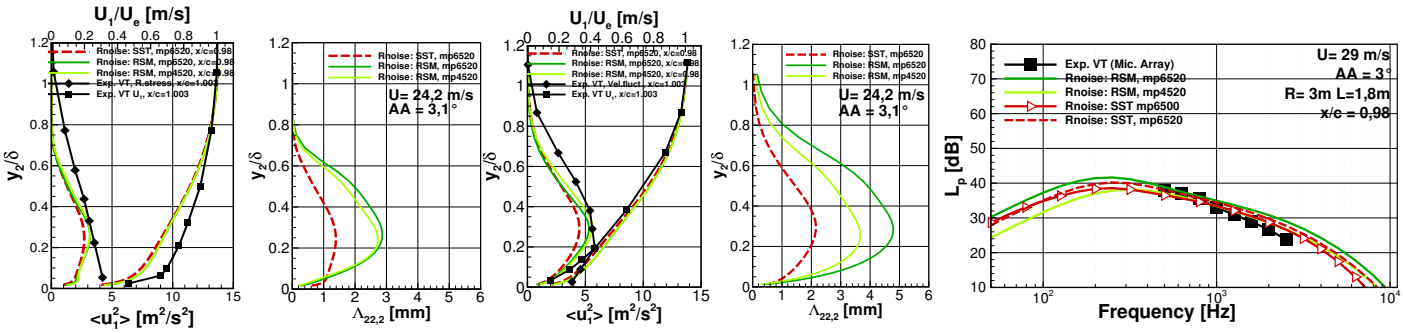

(a) $Re\ 1,69 \cdot 10^6$, without tripping, pressure side (left), suction side (middle) and total SPL (right).

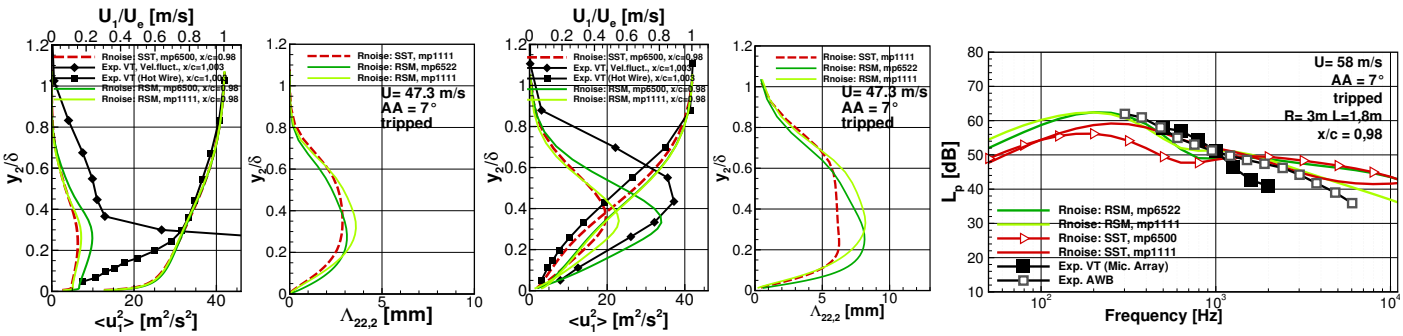

(b) $Re\ 3,15 \cdot 10^6$, with tripping, pressure side (left), suction side (middle) and total SPL (right).

Figure 3.2: Noise prediction results for DU96 airfoil

examinated are the ones less affected by these inconveniences, and required the prediction point location to be moved upstream.

For S831 airfoil no tripped cases are employable for comparison, for the reasons explained in Sec. 3.2.1. The character of the SPL agrees with the measured one (Fig.3.3b), and looks like for this airfoil the peak value lies at low frequencies, around 500Hz at the very lower limit the acoustic measurements are usually capable of. The turbulence models do not show a lot of difference, and for both the best fitting mode is mp6500. The BL measurements agrees very roughly and are generally underestimated by the prediction.

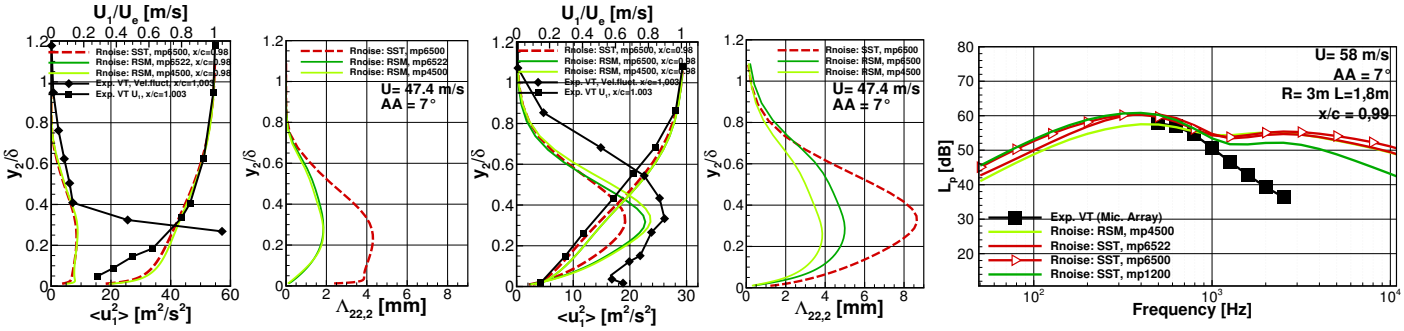

(a) Noise prediction results for DU96 airfoil, $Re\ 3,15 \cdot 10^6$, without tripping, pressure side (left), suction side (middle) and total SPL (right).

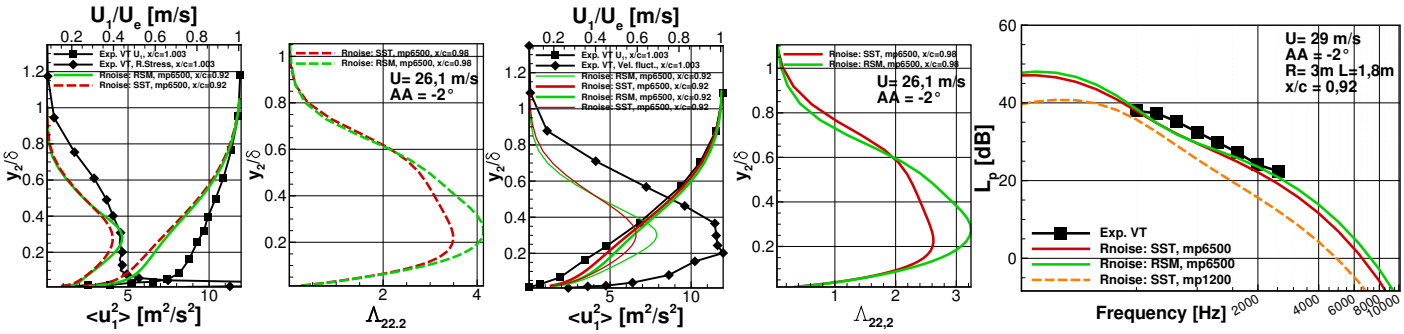

(b) Noise prediction results for S831 airfoil, $Re\ 1,5 \cdot 10^6$, without tripping, pressure side (left), suction side (middle) and total SPL (right).

The S822 airfoil noise is well predicted for 0°AoA with anisotropic modes (Fig.3.3c), while the isotropic ones clearly underestimate the levels, and the curve shape for the prediction falls too steeply on both sides. For 4°AoA (Fig.3.3d), the prediction becomes more difficult and looks like the anisotropic modes raise too much the levels resulting in an overprediction, but the curve shape is similar and is also nice to see in both measurements and prediction a slight two-peak shape is assumed. The restricted frequency measurement range, due to extraneous noise contamination, makes difficult to predict how the noise spectrum is made after the 3kHz.
For 8°AoA the agreement breaks totally (Fig.3.3e), and looks like in the experiments the measurement frequency range falls just between the two peaks, and the leftmost peak contribution from the ss has moved to even lower frequencies. A reason for this may almost surely lie in the prediction point, which has to moved fairly upstream due to a large recirculation zone resulted from the calculation at such high AoA, and in the high extraneous noise contamination, giving only 3 valid frequency band values.

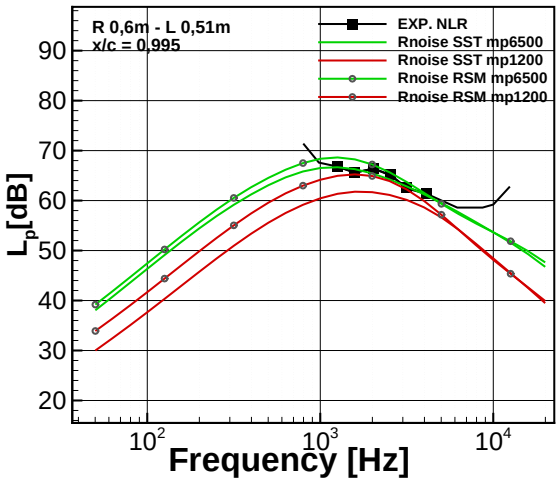

(c) 0°AoA.

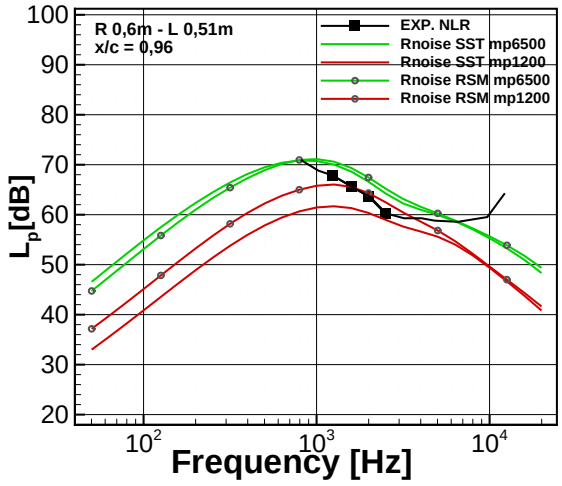

(d) 4°AoA.

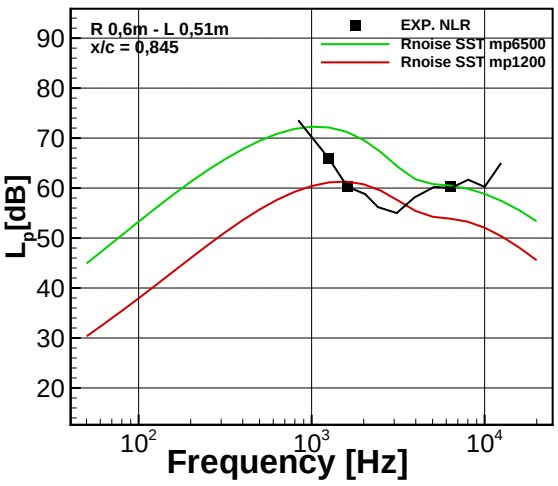

(e) 8°AoA.

Figure 3.3: Noise prediction results for S822 airfoil, $Re\ 1 \cdot 10^6$, with tripping. Unmarked black line indicates measurements considered invalid from the author.

For the S834 a converged solution could only be obtained for AoA 0°and 4°, since this profile was even more prone to recirculation than S822 and here again, the necessity to move the prediction point upstream out of the zone, making prediction less reliable. This is almost surely the reason why the main ss peak is always displaced more to the higher frequencies than in the experiment. For 0°the prediction is still not very far and differs in the best case at most by 4dB. For 4°AoA the agreement is already too decayed (Fig.3.4a, 3.4b). For this airfoil, the anisotropic calculation overestimates the results too.
It should be a good choice, in future experiments, to adopt always higher Reynolds numbers ($3 \cdot 10^6$ and above) and higher inflow speeds (50m/s and above) to ensure a good condition for this kind of aeroacoustic measurements, in order to achieve more stable BL and to better overcome the extraneous noise sources.

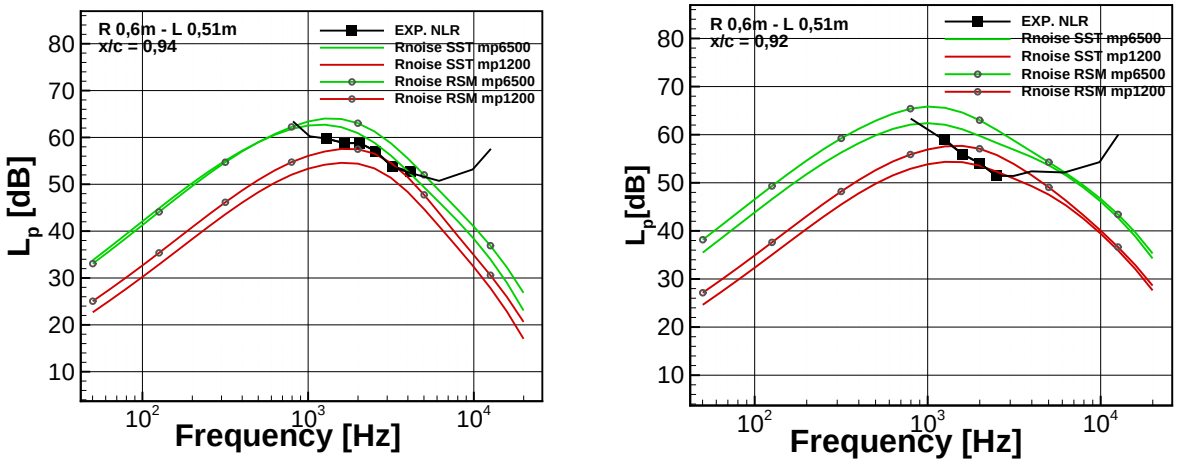

(a) 0°AoA.

(b) 4°AoA.

Figure 3.4: Noise prediction results for S834 airfoil, Re $0,75 \cdot 10^6$, with tripping. Unmarked black line indicates measurements considered invalid from the author.

The NACA63-215, for which the experimental data come from very different experimental setups, is clear example of the problems raising when experiments are conducted with uncommon setups. The main problem is that it is not known which of the many surface treatments were used while obtaining the data considered here. An array of vortex generators placed at 0,85c may have been used, feature which could alter substantially the scattered noise. At ca. 1,2kHz the experimental curve starts differing from the usual hill-shaped curve and continues rising for lower frequencies. The simulations done in fact shows fairly good agreement only in the 2-5kHz region (see Fig.3.5). The influence of the AoA in this case is very subtle, both on experimental and predicted results, in which the shape of the curve is preserved and levels higher (ca. 1,5dB more for higher AoA). The Reynolds number increase also leads in higher levels and the peak level is shifted to higher frequencies. The curve for the different modes shown are the ones which show the better agreement, and they are generally very similar to each other. The mp6500 mode always makes the exception and lies on higher levels by ca. 4dB. A difference between mp6500 and all the other selected modes is in having U_c set to the constant $0,7U_\infty$, resulting in these higher results. In regard to this, both measurements and predictions for this case suggest that this means to overestimate the noise levels.
The overall prediction is good and stable when the AoA is changed, but a question mark remains about how intense is the real TBL-TE noise at the lower frequencies and, thus, how near to the prediction it is.

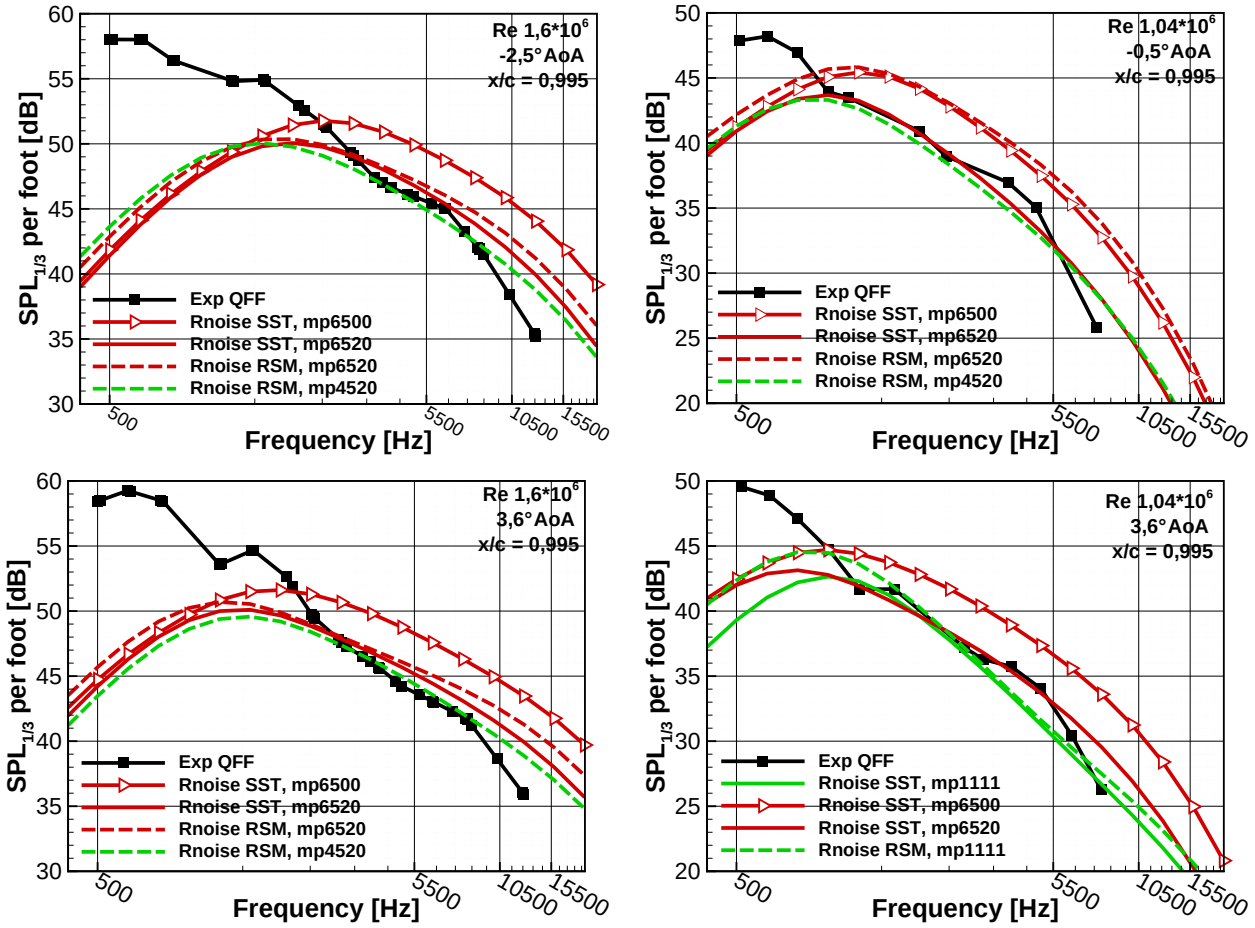

Figure 3.5: Noise prediction results for NACA63215 airfoil, without tripping. Left pictures: $Re\ 1,61 \cdot 10^6$, right pictures: $Re\ 1,04 \cdot 10^6$.

The SD2030 profile suffered for the very low Reynolds number in the experiment of $5 \cdot 10^5$, for which the 8°AoA case lead to total separation in the simulation. For the 0°AoA the experimental data are shaped as a more flat curve than the prediction one (Fig.3.6a). A remark has to be done here, since the measurement data in this case was clearly reported to be affected by extraneous noise sources which limits the measurements validity to a small "window" between 1–4kHz frequency. Therefore, even if the authors of the experiments tried to individuate which are the reliable data points, there still may be an influence of these on the "valid" measurements. Mostly, in the original plots, the data looks more like a valley than a hill, in which the reliable data lies between peaks clearly not of TBL-TE noise origin. The 4°AoA case has more agreement (Fig.3.6b) and the anisotropic models still seem to overpredict the measured noise.
The very low inflow speed chosen for this airfoil may be a cause of bad agreement, since the TBL-TE noise connected to such low speeds is also lowered. As the authors of the experiments indicate [31, Sec.3.3.4], the extraneous noise sources from model-endplate junction were quantified and data point affected for more than 1dB were discarded. But on p.11 of the same document they bring an example to show how anyway some points considered as good, are either way in consistent quantity affected by other noise sources, because in some cases the airfoil noise levels were too low. This condition makes hard to measure the noise produced by the airfoil only, because the SNR is likewise lowered.

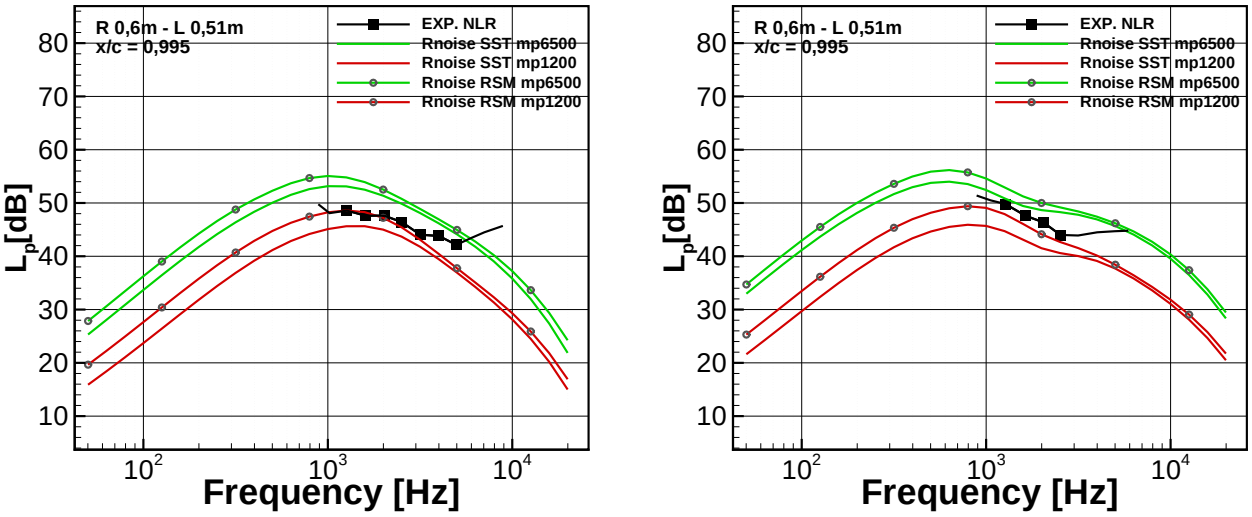

(a) 0°AoA. **(b)** 4°AoA.

Figure 3.6: Noise prediction results for SD2030 airfoil, *Re* $0,5 \cdot 10^6$, with tripping. Unmarked black line indicates measurements considered invalid from the author.

4 Active Flow Control Analysis

The AFC analysis have been carried adding a suction device on a portion of the airfoil surface, on which a constant pressure is attained which establishes the desired massflow. The same exact methodology described in 3.1 has been used, with the exception of a refined mesh in the proximity of the actuator position (Fig.4.1) and the particular FLOWer implementation which makes the simulation of the actuator possible. The tested cases start from the same conditions used by Wolf et al. [44] on a NACA64-418 airfoil. A description of the test facility utilized in the past experiments is given. A condensation of the tested conditions is shown and the obtained results are reported and analysed.

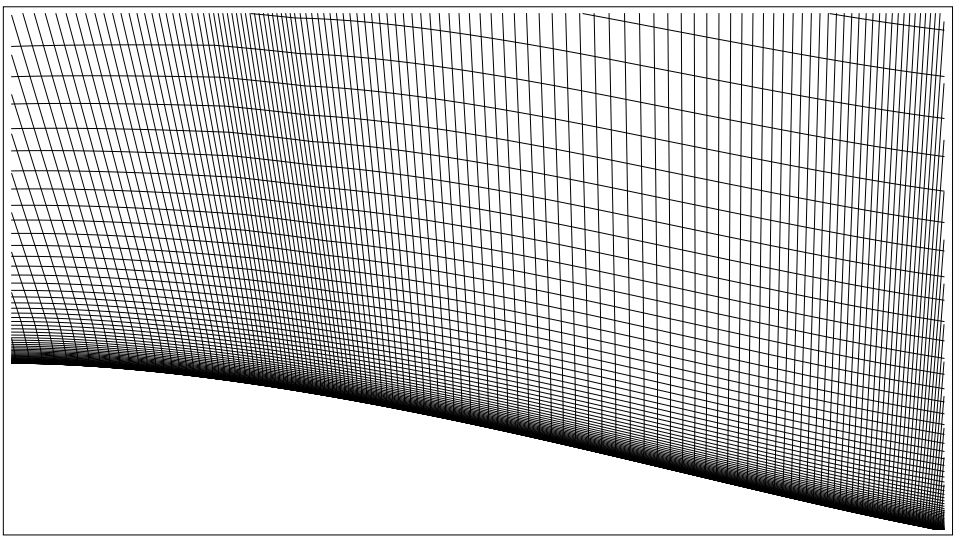

Figure 4.1: Example of mesh refinement for BL suction simulation. Base mesh is depicted in Fig.3.1

4.1 Description of the analysed cases

The flow conditions adopted here as a starting point (from now on, *default conditions*) are also the same used by in the experiments conducted by Wolf et al. [44], but here no comparison with them is made. These default conditions are: Re of $2,5 \cdot 10^6$, chord of 0,6m, U_∞ of 70m/s, M of 0,206, ρ of 1,064. It may be useful to recall the definition found in [40]

$$C_Q = \frac{Q}{\rho_\infty U_\infty S_s} \tag{4.1}$$

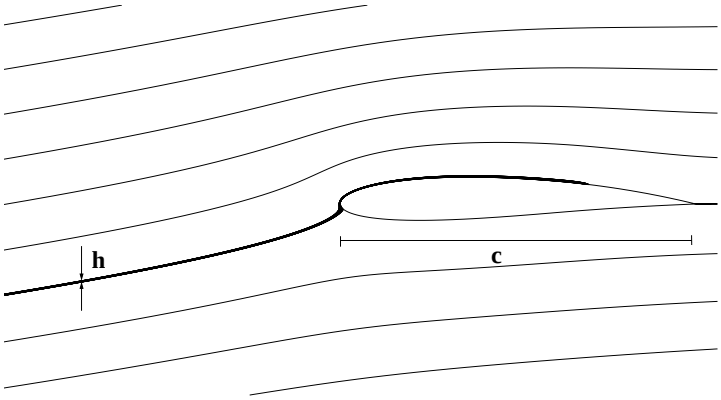

Figure 4.2: An explanation of Eq. 4.2 according to Schlichting [40].

Note that a Q of 0,12kg/s is assumed as default condition resulting in a C_Q of 0,073 which is ca. four times higher the maximum value adopted by Wolf et al. This is due to the use of only one 0,05c long actuator instead of four of them, but preserving of the same Q, thus emphasizing the effect of a single actuator. The suction surface S_s is referred to the total actuator surface (which is modelled in this work as a single open surface. It should not be altered even if one considers the effective open surface of a porous boundary). Another expression is available, also found in [40]

$$C_Q = \frac{h}{c} \tag{4.2}$$

Where h is the vertical thickness of the sucked layer at the infinity (see Fig.4.2). Another useful expression directly descending from Eqn.4.1 is

$$C_Q = \frac{v_s}{U_\infty} \tag{4.3}$$

Where v_s is the vertical velocity of the sucked flow over the actuator, assumed to be constant. The latter carries a more physical meaning, but unfortunately is not practically applicable since v_s is not constant and not known in advance. The parameter x_A will be used in this text to indicate the point of start of an actuator surface. This means that a value reported for $x_A = 0,25c$ is referred to a case with an actuator surface extending in the range of x/c 0,25–0,30. The conditions (x_A, airfoil, M, Re, C_Q, Q) have then been altered to investigate their influence, but always examining the effects produced by a single actuator of 5% chord length. The tested cases have been divided into 3 groups (see also Table 4.1):

Group 1: Starting test run at 3°and 6°AoA, with 0,12kg/s and 0,06kg/s of suction massflow. The actuator positions start from 0,25c chord at intervals of 0.1c until the last actuator starting at 0,85c is reached, resulting in 28 single simulations. The last actuator position is only of observational purposes since there will be likely not enough place into the airfoil where to place

the actuation devices. These conditions determine a C_Q of 0,073 and 0,037 for the two mass rates respectively.

Group 2: Basing on results from point 1, the same conditions are applied on NACA0012, 2212, 4212 and 2612 airfoils but only in the conditions of AoA 6°and Q 0,12kg/s have been considered, on positions starting from 0.45c.

Group 3: NACA64418 at 3°AoA with variation of flow and suction conditions. Two different Mach numbers chosen 0,26 and 0,15, keeping Re, C_Q constant at the same values of case 1. This implies different chord lengths and a lower and higher Q respectively.
NACA64418 at 3°AoA and two different Mach numbers 0,26 and 0,15, keeping Re and Q constant ($Q = 0,1kg/s$). This implies different chord length and a higher/lower C_Q respectively.
NACA64418 at 3°AoA and different Re numbers of $5 \cdot 10^6$ and $9 \cdot 10^6$, same U_∞ M and C_Q of default conditions, this implies in different chord lengths and Q.

4.2 Test matrix

It follows the condensation of the tested numerical cases, the aerodynamic characteristics of these airfoils is skipped since are largely available in literature. The cases are chosen to investigate the influence of various parameters, like airfoil shape, actuator position, maximum camber and its position, Mach number, Reynolds number, C_Q and Q.

Group, Airfoil	$Re \cdot 10^6$	M	α	c	U_∞	Q	C_Q	act range
Group 1 (M0)	2,5	0,206	3	0,6	70	0,06	0,073	25–85
(NACA64-418)	2,5	0,206	6	0,6	70	0,12	0,073	25–85
	2,5	0,206	3	0,6	70	0,06	0,073	25–85
	2,5	0,206	6	0,6	70	0,12	0,073	25–85
Group 2	2,5	0,206	6	0,6	70	0,12	0,073	45–85
(various airfoils)	2,5	0,206	6	0,6	70	0,12	0,073	45–85
	2,5	0,206	6	0,6	70	0,12	0,073	45–85
	2,5	0,206	6	0,6	70	0,12	0,073	45–85
Group 3 (M1)	2,5	0,26	3	0,48	88	0,077	0,073	45–85
(NACA64-418)(M2)	2,5	0,15	3	0,82	51	0,134	0,073	45–85
(M3)	2,5	0,26	3	0,48	88	0,1	0,094	45–85
(M4)	2,5	0,15	3	0,82	51	0,1	0,054	45–85
(M5)	2,5	0,26	3	0,48	88	0,1	0,123	75
(R5)	5	0,206	3	1,2	70	0,39	0,073	45–85
(R9)	9	0,206	3	1,2	70	1,27	0,073	45–85

Table 4.1: Test matrix of the investigated numerical simulations with AFC

4.3 AFC results and analysis

The most striking result obtained from all the calculations, in every condition, is that the position of a single actuator as it was modelled, is much less influential than expected. This is in contrast with the results found in literature aimed to better performances (Sec.2.4), where the optimal solution was found to concentrate suction in the forward part of the airfoil: it never happened in the simulations to get less overall noise prediction with x_A/c lower than 0,45. The better reduction in dB has never overcame 2% of the baseline value, and all the other solutions are tightly distributed under this value. Upon observing the development of the calculated TBL (Fig.4.3 shows two example cases), it can be found a substantial reduction in the BL thickness and its development, and the difference from the baseline builds up noticeably downstream of the actuator. The BL thickness is however not very representative of the potential noise generated. If thinking to realize a massflow balance between only the massflow in the entire BL at the beginning of the actuator, the massflow in the entire BL at the end of the actuator, and the massflow Q removed, this balance is not satisfied. This is due to the fact that the BL develops over the actuator surface, as also reported from experiments with suction in reference [43, p.7].
The other flow and turbulence parameters in the BL like $\frac{dU_1}{dy}$, Λ_2 and k_T are altered, typically having higher intensities in the near wall layers and lower in the outer layers. The effects on the resulting noise prediction are a good but not radical noise reduction, limited to 4-5dB. This suggests that the majority of the noise is bound to the very near wall layers of the BL, which develops again after the actuator has taken effect, and would require instead a less intense suction, but distributed over a longer surface. The velocity profile results also always fuller, implying a heightened derivative $\frac{dU_1}{dy}$ at the wall, becoming then lowered after a certain distance that has been found to be always less than $\delta/2$.

Besides from these general observation, a detailed look at the results of Group 1 calculations (Tab. 4.2) shows the presence of an optimal point at x_A/c 0,65, thus the very small difference from the neighbouring suggests it to be more a plateau of good conditions, that worsen after x_A/c 0,85 and before 0,55. Halving the Q, thus also the C_Q, doesn't bring different results, other than having a weaker noise reduction in all cases. Doubling the AoA, brings also almost the same results in

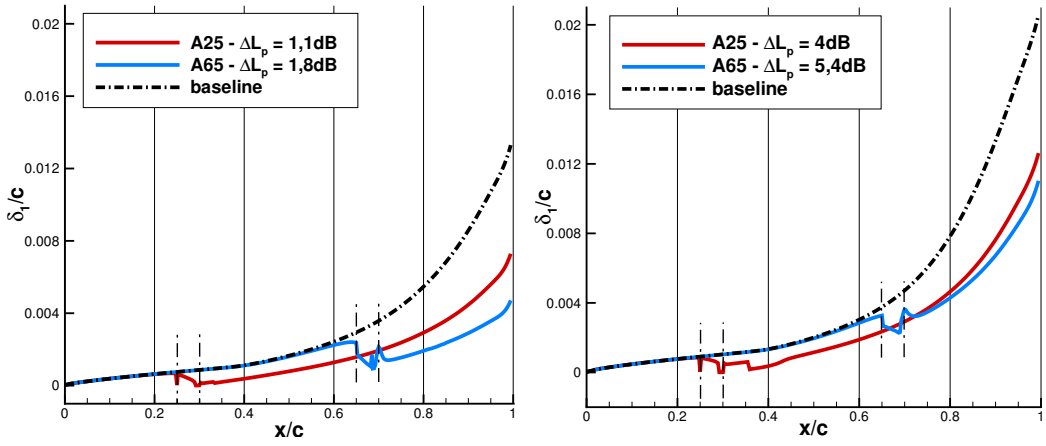

Figure 4.3: Example of typical development of $\frac{\delta_1}{c}$ on the suction side of an airfoil with actuator positioned at 0,25c and 0,65c. 3°AoA and 0,12kg/s of suction mass (left), 6°AoA and 0,06kg/s of suction mass (right). The predicted noise improvement is in relation with the respective baseline case.

Actuator Pos	Q = 0,06kg/s		Q = 0,12kg/s	
	L_p	ΔL_p	L_p	ΔL_p
25	71,71	0,8	71,4	1,1
35	71,45	1,1	71,21	1,3
45	71,17	1,3	70,92	1,6
55	70,97	**1,5**	70,74	**1,8**
65	70,94	**1,6**	70,69	**1,8**
75	71,18	1,3	70,78	1,7
85	71,8	0,7	71,1	1,4
baseline	72,5		–	

Actuator Pos	Q = 0,06kg/s		Q = 0,12kg/s	
	L_p	ΔL_p	L_p	ΔL_p
25	72,67	4	71,86	4,8
35	72,12	4,6	71,4	5,3
45	71,65	5	70,92	5,8
55	71,29	**5,4**	70,64	**6**
65	71,27	**5,4**	70,62	**6,1**
75	71,74	4,9	70,88	5,8
85	72,9	3,8	72,2	4,5
baseline	76,7		–	

Table 4.2: Results of Group 1 calculations for AoA 3°(left) and 6°(right). All results are referred to position 0,995c and all the reductions referred to the baseline (last row)

terms of optimal positions, and the noise reduction effect is stronger and thus can be regarded to be proportional to the baseline noise. This is linked to what previously stated, that even if for 3°the BL thickness is much smaller compared to the 6°cases, and consequently the relative amount of BL removed is higher, the impact on noise reduction does not follow this logic, and is in some cases unexpectedly weaker when the relative amount of BL removed is higher.

This is more clearly noticeable from the results in Fig. 4.4, where the solid lines reports the obtained reduction in dB and shows the mentioned optimal point, or plateau, between 0,55c and 0,65c positions. it is important to note that this figure is oriented to the reduction of the parameters respect to the baseline values, and not their absolute value. The *BLR* acronym stays for boundary layer reduction, meaning the percentage of the employed mass flow Q against the total mass flow in the BL at the beginning point of the actuator. It is always decreasing, being the BL thickness always increasing going downstream, and reaches values of 70% in the most favourable situation of maximal Q, minimum AoA and most upstream actuator position. It is intended to show how this value can not explain the optimal position found for the actuator. The remaining marked lines show the ratios between the BL thickness obtained in the observed case and the respective baseline case ($\frac{\delta}{\delta_b}$). The observed point is in proximity of the TE at 0,99c and the calculation is made for every actuator position. A relation between reduction of δ_1 and reduction of overall noise is visible.
The minimum values of the thickness ratio looks like moving downstream for Q = 0,12kg/s, but, like the other parameters, the difference is very subtle. For all the parameters, with the higher mass flow the curves are steeper and shifted to higher values, however the result on SPL reduction is the same, except for a constant proportional to the AoA.

After these results, other different airfoils shapes have been tested, to search whether the airfoil shape influence the position of the optimal point or not. Different 4-digit NACA airfoils have been chosen due to the easy way the main parameters of maximum camber and maximum camber position can be changed. For this airfoil family the first digit indicates the position, in tenths of chord, of the x-point of maximum camber, and the second digit indicates the maximum camber in chord percent. The results in Fig. 4.5 shows the reduction of SPL for these four airfoils (relative to the respective baseline cases), in function of the actuator position. Because the only result to investigate is the optimum position, only the values x_A/c 0,45–0,85 have been simulated. It shows the same tendency encountered for the NACA64-418, of having more reduction on thicker BL (all conditions are identical), in this case originated by higher maximum camber. The moving of the maximum cam-

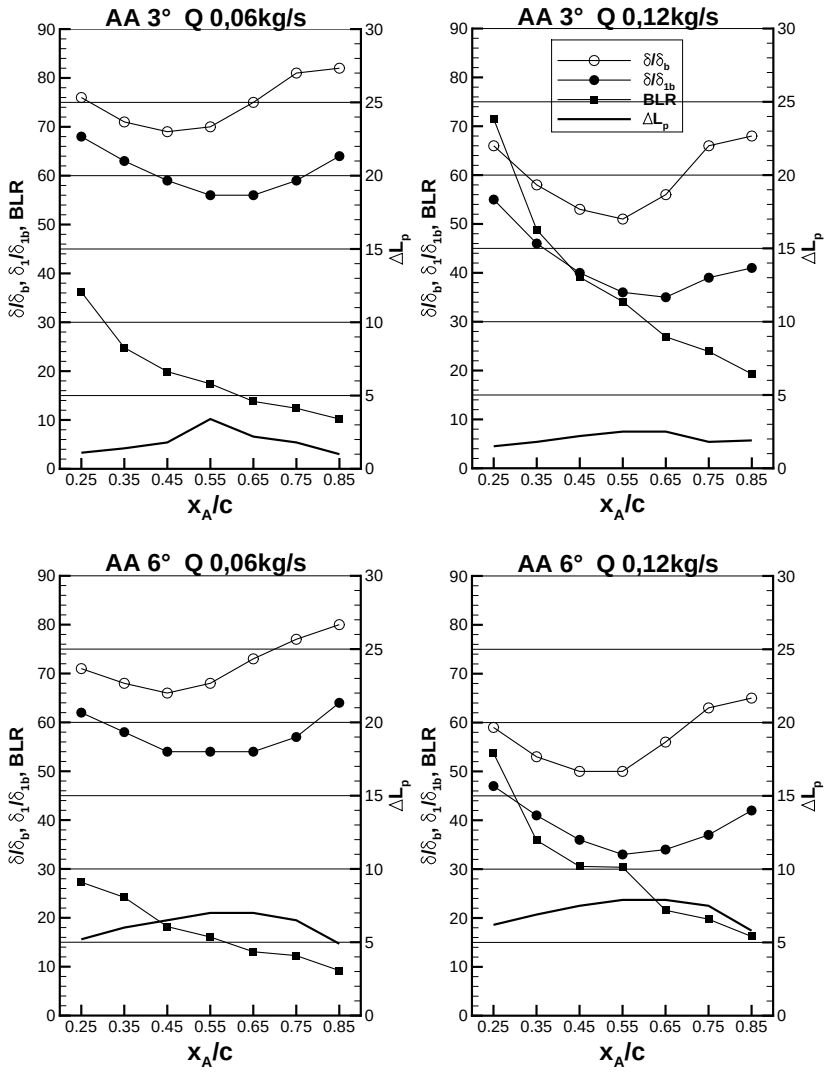

Figure 4.4: Ratio of BL thickness of cases from Group 1 respect to the baseline condition, BLR is the ratio of BL going to be removed, measured at the position just before the actuator

ber towards the TE moves the optimal point very slightly towards x_A/c 0,75, but raises even more the obtained reduction. To obtain a further confirmation of this dependence of the noise reduction amount on the higher max camber and camber position, a single test with a DU96 airfoil has been made, for x_A/c 0,75. DU96 has 2,5% max camber at 0,36c position. The noise reduction has been predicted to be 2,53dB which seems to be in agreement with the hypothesis, since the max camber is lower than the one of NACA4212, but its position value is higher. Likewise, the max camber is higher than the one of NACA2612 but its position value is lower in comparison to it. The point for DU96 lies between the two NACA airfoil results.

The BL thickness δ at the TE has shown (Fig.4.4) to be not directly linked to the the resulting noise. Other parameters in the BL have been investigated, and the most responding factor found was the turbulent kinetic energy k_T. Figs. from 4.6 to 4.9 depict the typical development of k_T plotted against the y dimensional distance from the wall, to show the proportions it assumes along the airfoil. Conditions in these pictures are always the *default conditions* with 6°AoA and Q =

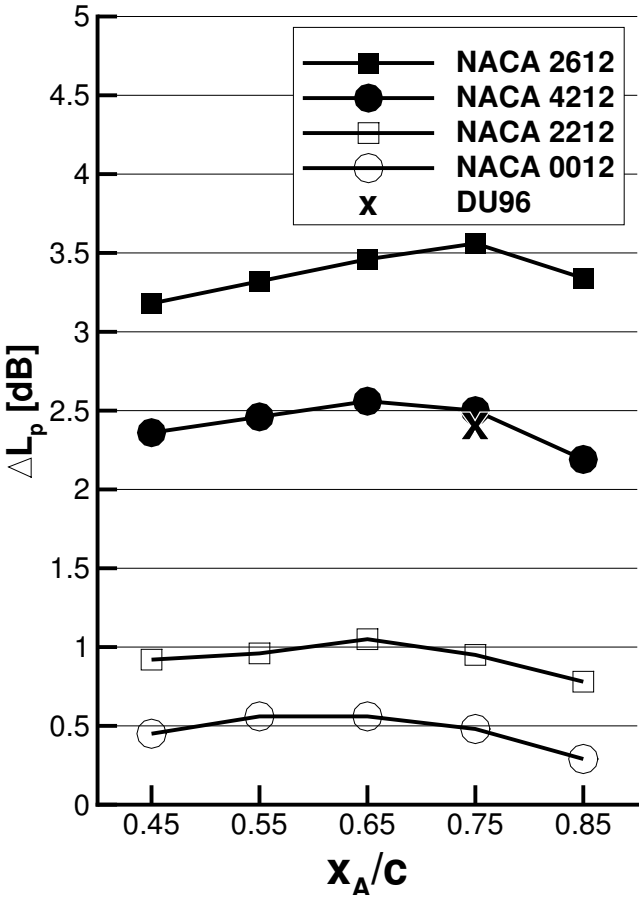

Figure 4.5: SPL reduction respect to the relative baseline cases for four NACA airfoils at same flow conditions

0,12kg/s. Different lines indicates the different actuator position cases, thus the chosen positions must not be over and too close to the ones covered by the actuator in each case, to make sure that sudden fluid variations have faded. The dashed lines indicates that in the corresponding case the actuator has not yet been encountered at that position. All the BL parameters look almost the same compared to the baseline, until the distance of 0,1c upstream of the actuator is reached. After this point the presence of the actuator starts to influence the BL conformation. Closer after the actuator a strong peak is added to the k_T profiles for all examined airfoils, except when x_A/c is greater than 0,65 and only a small increase is found. This peak then fades within the rest of the distribution after some distance (around 0,15c). A not yet demonstrated explanation for this phenomenon regards the layer of fluid that comes to take the place of the sucked layer, which possesses a higher momentum and needs to flow longer on the surface to be slowed down at the typical speeds in the BL, thus this higher momentum becomes visible in the BL profile.
Beside this peculiarity, it can be seen from the figures that the BL grows again after the actuator and so does the k_T in its medium and peak value, but the trend is that the more downstream the actuator is placed, the slower the BL recovers its turbulence. The most remarkable conclusion is that the benefits of the actuator starts really to take effect at a certain distance to the actuation point, thus not right after it. This benefit can be explained by observing that the BL develops slower after an actuator positioned more downstream. For example, in Fig.4.9 the curves for A45 and A55 at 0.83c position indicate a better solution and A75 is worse. But A75 indicates a slower development and gets exceeded in a short distance by the previous two solutions, thus becomes better at the

point where the noise is scattered. A85, instead, is worse after the actuator and remains worse since the TE is right at a short distance after it, and the distance at which its advantages take place is greater than the distance from the TE.

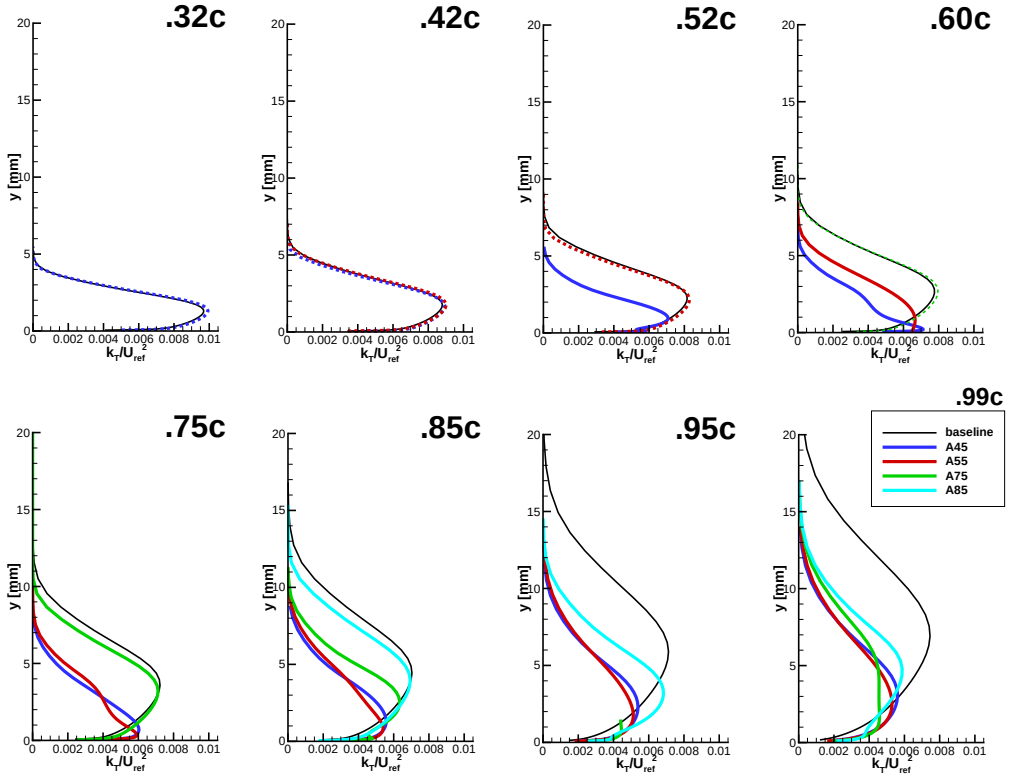

Figure 4.6: Profiles of k_T for NACA2612 along various positions, with lines indicating actuation at different positions. Dashed lines indicates that for the corresponding case the actuation has not yet taken effect at that chord position.

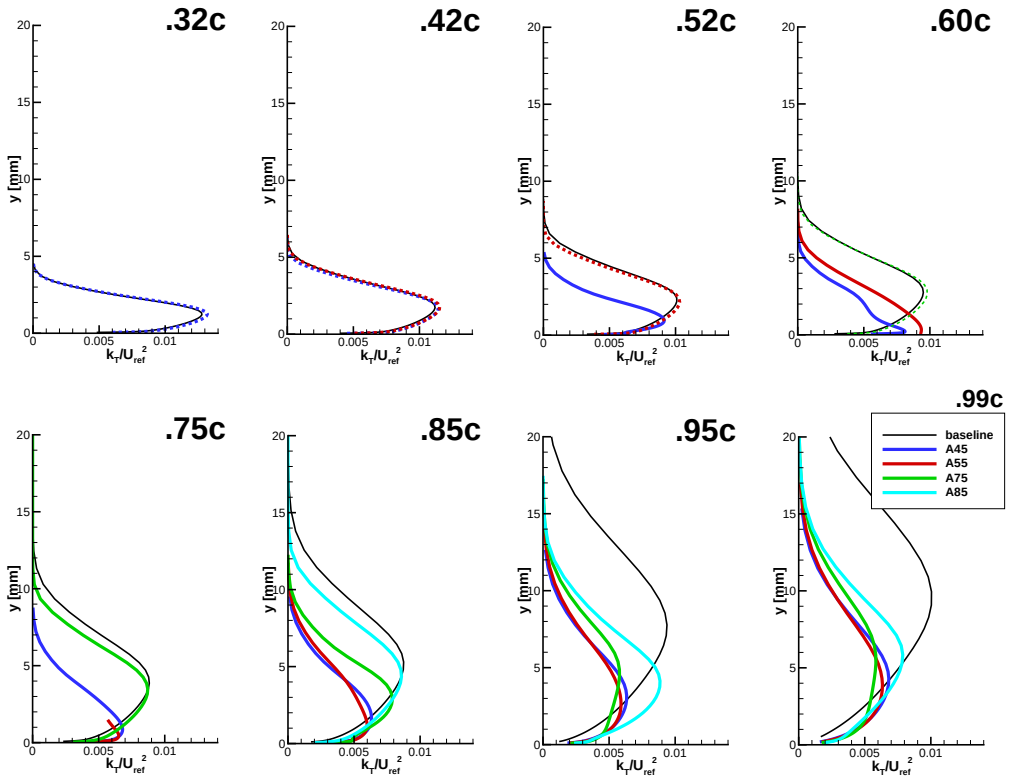

Figure 4.7: Profiles of k_T for NACA2612 along various positions, with lines indicating actuation at different positions. Dashed lines indicates that for the corresponding case the actuation has not yet taken effect at that chord position.

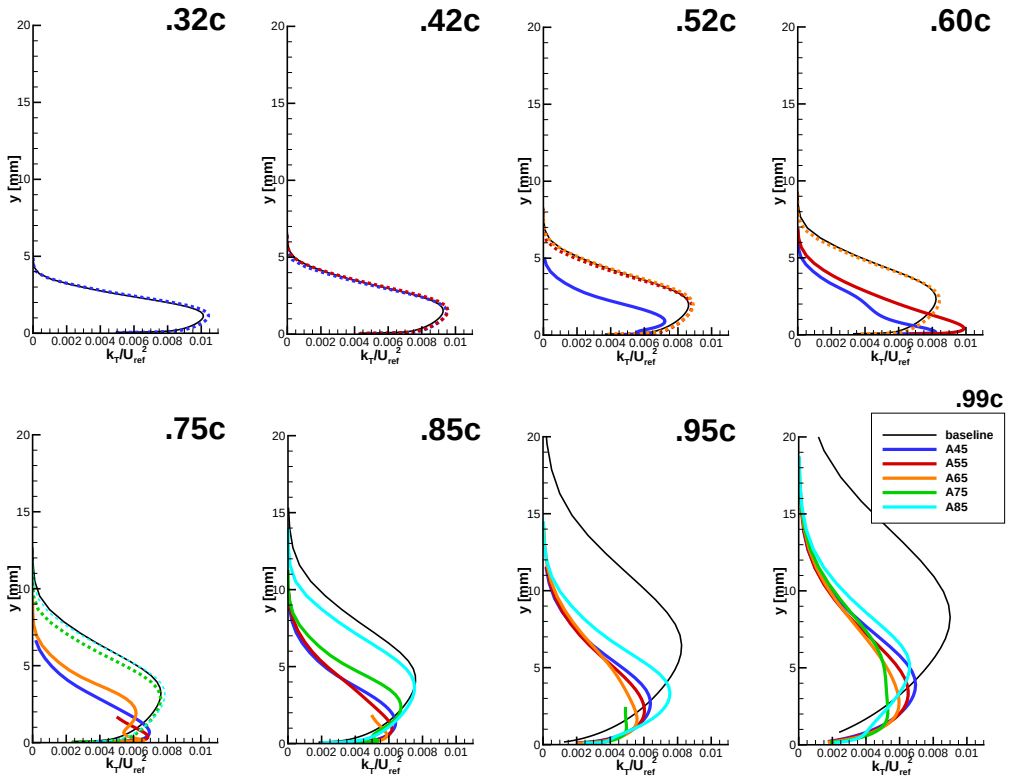

Figure 4.8: Profiles of k_T for NACA2612 along various positions, with lines indicating actuation at different positions. Dashed lines indicates that for the corresponding case the actuation has not yet taken effect at that chord position.

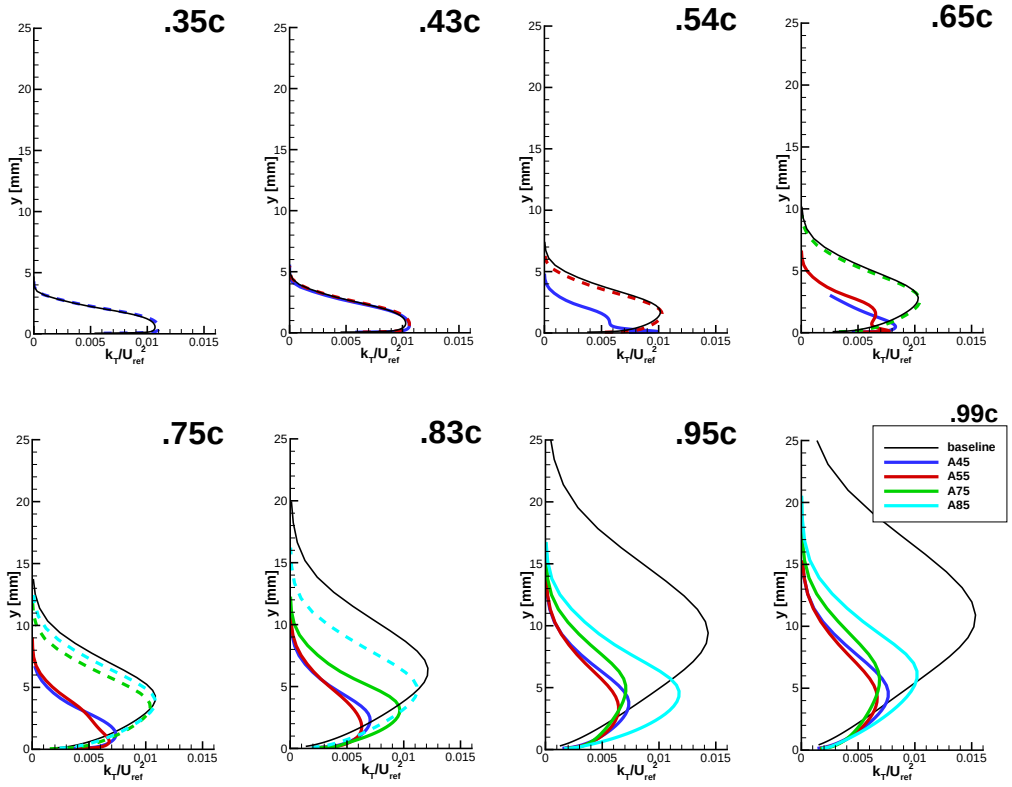

Figure 4.9: Profiles of k_T for NACA64418 along various positions, with lines indicating actuation at different positions. Dashed lines indicates that for the corresponding case the actuation has not yet taken effect at that chord position.

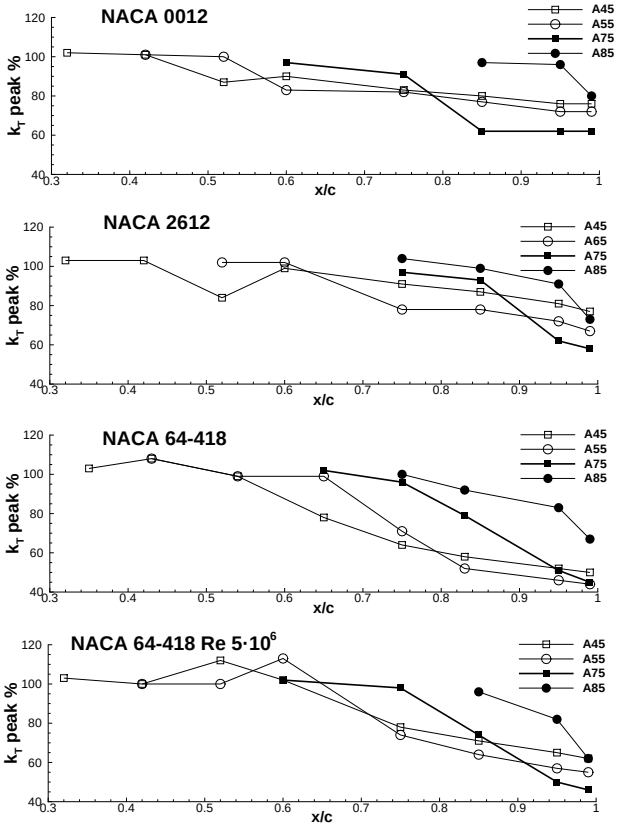

Figure 4.10: Ratio of k_T profile peak respect to the relative baseline cases for different NACA airfoils at same flow conditions

This conclusion can be proved with a deeper examination of these graphs, measuring the absolute peak value of the k_T profiles, in relation to the values of the baseline case. Fig.4.10 shows that this parameter is well related to the overall noise emission. After the suction takes effect, the peak of the turbulence kinetic energy (which anyway is always growing in its absolute value) grows slower than in the baseline case, and the more downstream the suction is applied, the stronger is the effect. But it happens that for actuator positioned too downstream the point of highest reduction would be placed *after* the TE, and thus it is not reached. This leads to an optimal suction position between x_A/c 0,55 and 0,75 from which the outcome is almost the same. This effect has been observed also for a higher Re.

It follows that, the outcome may have been the same for all the observed cases, because the inflow conditions were the same. In the Group 3 case run, the values of M, Re, Q and C_Q have been individually altered in search for correlated effects. For all the simulations now on, the actuator positions x_A/c 0,45–0,85 have been considered. The first two conditions (M1 and M2) have only the inflow Mach number varied, resulting in a different chord and Q value to realize this, since Re is constant. The third and fourth (M3 and M4) have M varied in the same way as M1 and M2, but keeping Q constant instead of C_Q (see Tab.4.1). In this way only the relation between v_S and U_∞ is expected to change.
When looking at the results, the different cases are always compared with the same M0 case, which still employs actuation and is drawn with black lines. The baseline values, different for each case, are always reported with dashed lines.

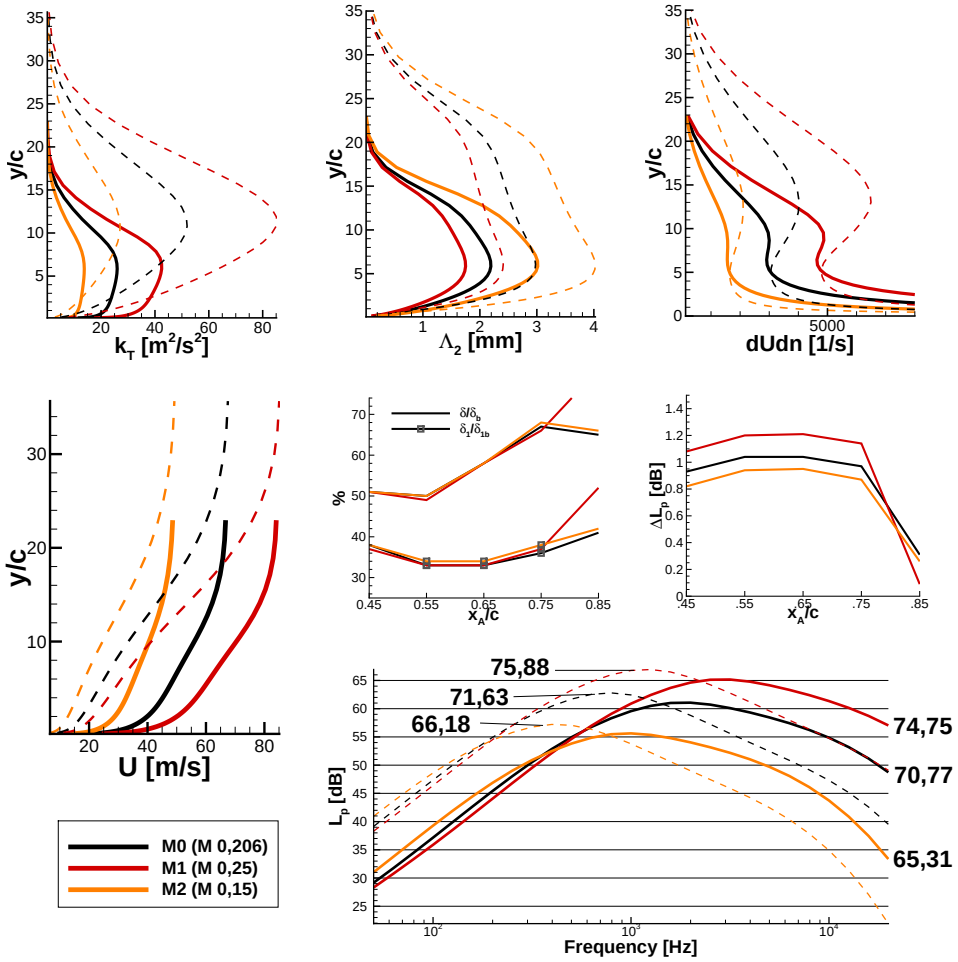

Figure 4.11: Effects of Mach number variation. M0,M1,M2 labels in Tab.4.1, read text for a correct interpretation.

It is always important to remark that the focus is on the *reduction* of SPL, instead of its absolute values. Thus, examining Fig.4.11, even if total SPL for case M1 is higher, the reduction for it is higher (middle-right plot). The three topmost plots displays the BL parameters (at x/c 0,95, for the cases with actuator positioned at x/c 0,75), which are related to the subsequent noise calculation (bottom plot). The velocity profile reported is extracted near the TE at the same position x/c 0,95, and the central plots reports the relative reduction of δ and δ_1 and the absolute reduction of noise, ΔL_p.

k_T **plot:** Here it is shown how the BL thickness compared to the respective chords is the same, but the intensity of the values is higher because of higher inflow velocities. The values are higher for higher Mach numbers, and the curve shapes are similar. The peak values have been measured and it has been noticed that the reduction in respect to the relative baseline cases is always 50%. This feature is connected to the employment of always the same C_Q. This implies that the difference between the cases with suction and their baseline is then higher for higher Mach numbers, leading to a higher noise reduction. It is also noticeable the double effect of slight increase in the very near wall distance, and noticeable reduction in the remaining zone.

Λ_2 **plot:** This parameter behaves in the opposite sense of the previous, showing decreasing values for higher Mach numbers. This has, however, less influence in the noise calculation and it can be seen the peak values are attained at decreasing wall distances for increasing Mach numbers. This means eventually shifting the noise frequencies to higher values, which contribute less to the total SPL than lower frequencies.

$\frac{dU_1}{dn}$ **plot:** This parameter behaves in the same manner as k_T, and the same considerations are here applicable. This parameter has, however, much more influence on the total noise spectrum (see Eq. 2.3).

$\frac{\delta}{\delta_b}$, $\frac{\delta_1}{\delta_{1b}}$ **plot:** This plot is intended to find a relation between the actuator position which leads to the lowest noise emission and simply the BL thickness and momentum displacement thickness at the TE. It shows that there is no relation with BL thickness, whose reduction is always less moving the actuator downstream (ratio is always done with the corresponding baseline, subscript b). A little relation is found with the momentum displacement thickness reduction, but the variations are still too small for deducing a conclusion. Notice that for increasing Mach number, the absolute values of δ_1 are higher, the δ_1/c values coincide and the ratio with baseline (which this plot shows) are also pretty unchanged, if exception is made for the last actuator position, which is deemed to be too far downstream and letting the flow changes introduced to interact negatively at the trailing edge.

BL velocity profile: The velocity profiles of the baselines are similar and only scaled to higher velocities when M is increased, the BL thickness referenced to the chords is the same and the cases with actuator show the same behaviour, with a more marked difference between them when the Mach number is increased.

The results in Fig.4.12 are useful to see the effect of having C_Q varied for the situation observed in Fig.4.11. The bottom SPL plot shows the noise spectrum and total SPL, for which the behaviour can be explained by the accompanying plots. A case with even higher C_Q is evaluated only for the 0,75c position (labelled M5), which is in fact the same as M3 but with $C_Q = 0,123$: it shows that an even intense suction leads to almost no improvement in SPL reduction and a reversal in the trend of k_T and $\frac{dU_1}{dn}$. This suggests that a limit coefficient of suction exists, beyond which the effect are generally negative.

k_T **plot:** The BL thickness compared to the respective chords is still the same, and the intensity of the values is higher because of higher inflow velocities. But in this case the curve shapes are not similar, and the increase of C_Q adds a even stronger additive contribution in the wall distance under 3mm. The peak values have also been measured and the reduction amount respect to the baseline is not anymore 50%, but slightly higher when C_Q is higher. This means that the same positive effects found for M1 are in this way even enhanced (as expectable) but some concerns may rise around the increased values near the wall, which with higher values of C_Q looks producing overshoots that could explain the deterioration of noise reduction.

Λ_2 **plot:** This shows the same behaviour as the previous M1, M2 cases, with the difference that here also the curve shape is altered and higher C_Q seems to lead to a concentration of the distribution, towards a shape more similar to a bell.

$\frac{dU_1}{dn}$ **plot:** The same observations made for k_T apply.

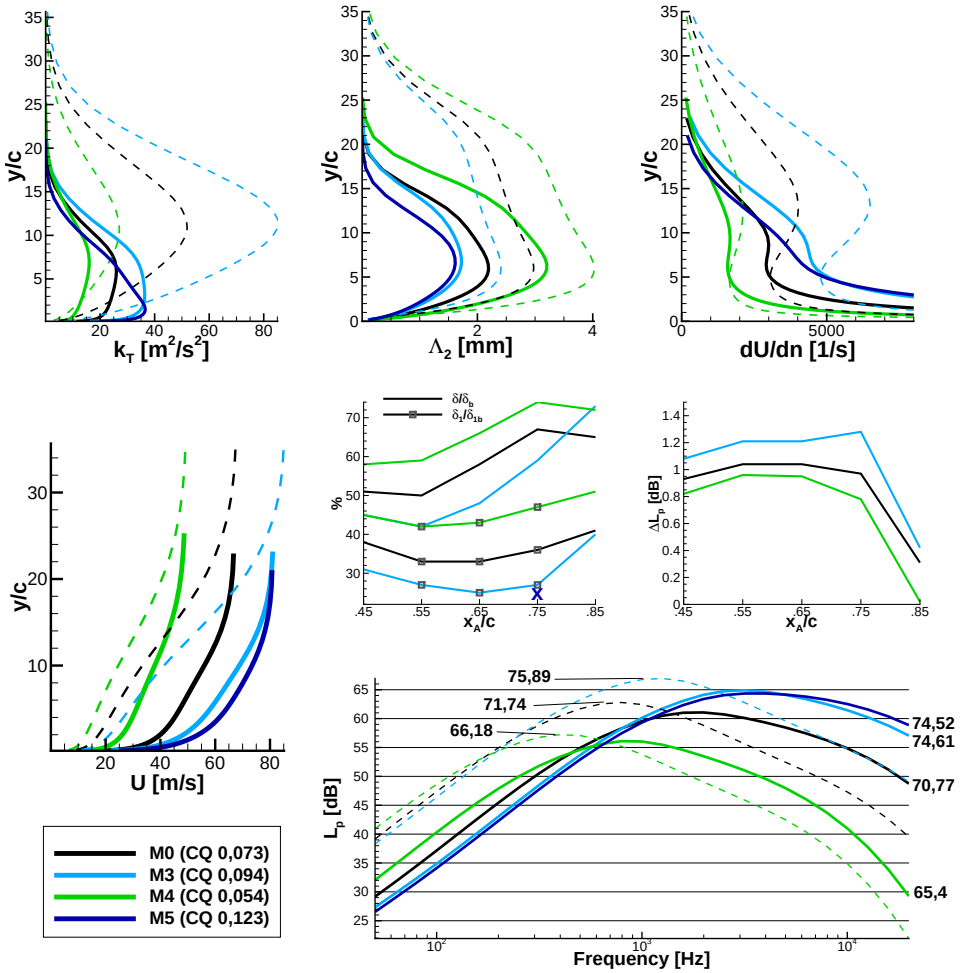

Figure 4.12: Effects of Mach number and C_Q variation. M0,M3,M4 labels in Tab.4.1, read text for a correct interpretation.

$\frac{\delta}{\delta_b}$, $\frac{\delta_1}{\delta_{1b}}$ **plot:** In this case the reductions in the values looks almost constantly offset from each other. The reduction ratio here is clearly higher when the C_Q is higher. The "x" symbol reports the value for M5 at 0,75c and shows little or no reduction, in spite of the greatly increased C_Q.

BL velocity profile: The velocity profiles get modified in the same way as in Fig.4.11, but they look even fuller when C_Q is higher. The curve for $C_Q = 0,123$ does not differ very much from the one with $C_Q = 0,94$.

The results in Fig.4.13 leads to useful observations, having the C_Q back again restored to the default condition of 0,073 and only Re varied. The bottom SPL plot shows the noise spectrum and total SPL, which happens to be lower for increasing Re. However, the increase in Re from 2,5 to 5 millions causes a little decrease in SPL of 0,7 dB, while the spectrum peak is shifted to lower frequencies and lower levels. The further increase from 5 to 9 millions causes the same (or even weaker) variation in the SPL, thus the sensitivity to Re seems strongly reducing when the number is increased, suggesting an asymptotic limit for the reduction. The relative SPL reduction, however, shows that the benefit is drastically decreased more than linearly with Re. Looking at the accompanying plots, it can be

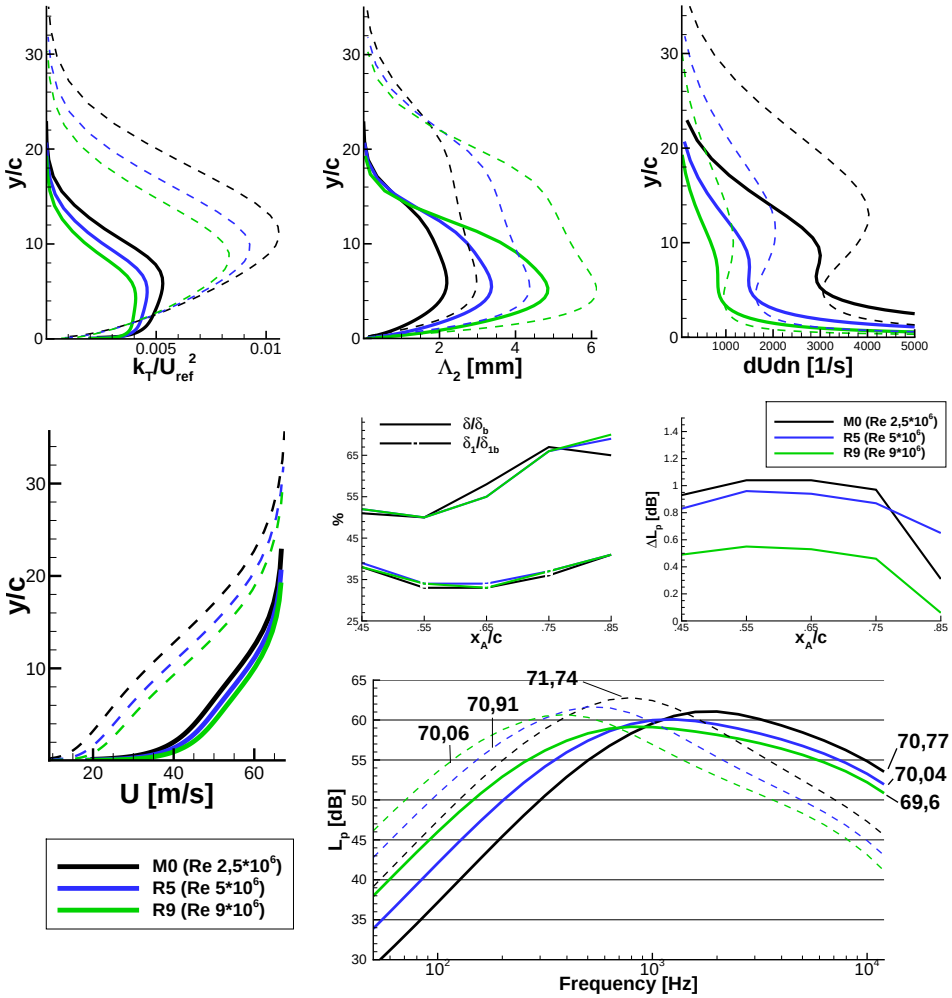

Figure 4.13: Effects of Reynolds number variation. R5,R9,M0 labels in Tab.4.1, read text for a correct interpretation.

deduced that:

k_T **plot:** The BL thickness compared to the respective chords now are not the same, as expected from the basic BL theory. The intensity of the values is lower for increasing Reynolds numbers, but the reduction (calculated measuring the value at the peaks) happens again to be at 50%. This is a qualitative observation which shows the similarity of effect obtained when C_Q is maintained the same.

Λ_2 **plot:** This plot shows curves behaving the opposite sense of the other two plots, like already happened in Fig.4.12 and 4.11. The increase in Re is accompanied by a strong increase in the peaks level. The peak values are also reached at lower distances from the wall for increasing Re. This is currently not immediate to see, but it is more accentuated when using a y scale instead of y/c.

$\frac{dU_1}{dn}$ **plot:** The same observations made for k_T apply, and here the weaker reduction respect to the baseline for increasing Re is clear to see.

$\frac{\delta}{\delta_b}$, $\frac{\delta_1}{\delta_{1b}}$ **plot:** This plot shows clearly that the different BL developed at different Re obtain the same exact reduction. This is interesting since shows how the reduction of the BL thickness is only function of C_Q, and it is not a sufficient parameter to determine which solution is quieter.

BL velocity profiles: The velocity profiles become fuller in a similar fashion, the shape is not changed when Re is increased, but only shifted to higher velocity values of an amount which is decreasing with increasing Re, suggesting the presence of an asymptotic, maximal effect.

5 Conclusion

For this thesis having two connected objectives, validation and search for new results, different conclusion can be deduced about the work made.
For the validation objective, it can stated that validating TBL-TE noise predictions is difficult due to the many unknowns in the measurement conditions. Another problem connected to this is that experiments do not often report all the exact flow conditions attained during the tests, and the same goes for tripping conditions and external noise contamination. A higher Reynolds number to choose for the tests is also always to prefer.
All the documents found so far do not show care taken for these aspects, and often the results are fragmented and different between them, especially the measurements frequency range which is often very different between different experiments authors. The predictions done with Rnoise have shown better correspondence when the airfoil is far from its maximum c_l. The consideration of anisotropic turbulence leads to higher SPL predictions, which in most of the cases have shown to be closer to the measurements. About the results of experimentations with ANC, it has been deduced that, according to the simulations, suction of small quantities of flow away from the boundary layer is an effective solution to reduce TBL-TE noise. How intense is the required energy consumption, and how severe is the effect of pressure loss through the porous plate is still to be determined. Another important aspect to consider in future works is the development of the boundary layer over the actuator surface itself, since in the adopted methodology no solid boundary represents the actuator surface.
In the examinated case of a short length actuator, some sudden variations are imposed to the flow in the boundary layer and in the outer flow field. The improvements are limited to 4–5dB when the suction mass is at its highest reasonable values. This, along with other results, suggests that a more distributed suction surface may be more effective than a concentrated one. The concentrated actuator resulted to be not very sensitive to the inflow conditions, and improves its effects only when the boundary layer turbulence intensity is higher and the suction massflow is higher (until a upper limit for it is reached).
It has also been observed, upon varying the Reynolds number only, that a practical wind turbine application, where the chord Reynolds number is expected to be higher, may represent an unfavourable condition for the effectiveness of BL suction.

Appendix

Airfoil Characteristics

Airfoil	t_{max}/c %	camber$_{max}/c$ %	C$_{Lmax}$
DU96	18	2,5	1,3
S831	18	5,1	1,3
S822	16	1,9	1,4
S834	15	1,6	1,3
SD2030	8,6	2,2	1,4
NACA63-215	15	1,1	1,41
NACA64-418	17,8	2,1	1,35

Table 5.1: Aerodynamic characteristics of employed airfoils for experimental data validation, values referred at Re 1.510^6

Bibliography

[1] R. K. Amiet: *Noise due to turbulent flow past a trailing edge.* Journal of Sound Vibration, Vol. 47, No. 8, P. 387–393, August 1976.

[2] CFD Group TU Berlin. http://www.cfd.tu-berlin.de/index.php?sec=research.

[3] F. Bertagnolio, H. Aa. Madsen and C. Bak: *Comparison and validation of trailing edge noise models.* In: Wind Turbine Noise-2009, Aalborg, Denmark, jun 2009.

[4] W. Blake: *Mechanics of Flow-Induced Sound and Vibration Vol. I and II.* Academic Press, Orlando, 1986.

[5] T. F. Brooks, D. S. Pope and M. A. Marcolini: *Airfoil self-noise and prediction.* NASA Scientific and Technical Information Division, 1989.

[6] D. Coles: *The law of the wake in the turbulent boundary layers.* J. Fluid Mechanics, Vol. 1, No. 2, P. 191–226, 1956.

[7] T. Colonius and S. K. Lele: *Computational aeroacoustics: progress on nonlinear problems of sound generation.* Progress in Aerospace Sciences, Vol. 40, No. 6, P. 345–416, 2004.

[8] G. M. Corcos: *The structure of the turbulent pressure field in boundary-layer flows.* Journal of Fluid Mechanics, Vol. 18, No. 3, P. 353–378, 1964.

[9] W.J. Devenport, R.A. Burdisso, H.E. Camargo, E.D. Crede, M.C. Remillieux, M. Rasnick and P. Van Seeters: *Aeroacustic Testing of Wind Turbine Airfoils.* tech. rep., Virginia Polytechnic Institute and State University Blacksburg, Virginia, 2008.

[10] D.M.Chase: *Sound radiated by turbulent flow off a rigid half-plane as obtained from a wavevector spectrum of hydrodynamic pressure.* The Journal of the Acoustical Society of America, Vol. 52, No. 3, P. 1011–1023, 1972.

[11] Mark Drela: *XFOIL – An analysis and design system for low Reynolds number airfoils.* Low Reynolds Number Aerodynamics, 5-7 June 1989.

[12] M. Gad-El-Hak and R. F. Blackwelder: *Selective suction for controlling bursting events in a boundary layer.* AIAA Journal, Vol. 27, No. 3, P. 308–314, 1989.

[13] M. Goody: *Empirical Spectral Model of Surface Pressure Fluctuations.* AIAA Journal, Vol. 42, No. 9, P. 1788–1794, 2004.

[14] Y. Guo: *Acoustic analysis of low-noise actuator design for active flow control.* Journal of Sound

Vibration, Vol. 311, No. 04, P. 843–860, 2008.

[15] G.V.Lachmann: *Boundary Layer and Flow Control.* Pergamon, 1961.

[16] A. Hatzipanagiotou. Study thesis, IAG University of Stuttgart, 2012.

[17] M. Herr, C. Appel, J. Dierke and R. Ewert: *Trailing-Edge Noise Data Quality Assessment for CAA Validation.* AIAA Paper 2010-3877, 2010.

[18] A. Herring, M. Kamruzzaman, W. Würz, Th. Lutz and E. Krämer: *Design and wind-tunnel verification of low-noise airfoils for wind turbines.* AIAA Journal, Vol. 45, No. 4, P. 779–792, 2007.

[19] M. S. Howe: *A review of the theory of trailing edge noise.* Journal of Sound Vibration, Vol. 61, No. 12, P. 437–465, 1978.

[20] F. Hutcheson and T. Brooks: *Effects of Angle of Attack and Velocity on Trailing Edge Noise.* In: 42nd AIAA Aerospace Sciences Meeting and Exhibit, Reno, Nevada, Jan. 5-8, 2004.

[21] Anthoine J., Remmler S and Moreau S.: *Computation of Wall Pressure Spectra from Steady Flow Data for Noise Prediction.* AIAA Journal, Vol. 48, No. 9, P. 1997–2007, 2010.

[22] M. Kamruzzaman: *Study of Turbulence Anisotropy and Its Impact on Flow Induced Noise Emission.* Dissertation, University of Stuttgart, 2012.

[23] M. Kamruzzaman, A. Herrig, Th. Lutz, W.Würz, E. Krämer and S. Wagner: *Comprehensive evaluation and assessment of trailing edge noise prediction based on dedicated measurements.* Noise Control Journal, Vol. 59, No. 1, 2011.

[24] M. Kamruzzaman, Th. Lutz, A. Herrig and E. Krämer: *Semi-Empirical Modeling of Turbulent Anisotropy for Airfoil Self-Noise Predictions.* AIAA Journal, Vol. 50, No. 1, 2012.

[25] R. Kosin: *Laminar flow control by suction as applied to the X-21a airplane.* AIAA-1964-284 - AIAA 1ST Annual Meeting, Washington D.C., Jun 29- Jul 2, 1964.

[26] R. H. Kraichnan: *Pressure Fluctuations in Turbulent Flow over a Flat Plate.* Acoustical Society of America Journal, Vol. 28, No. 3, P. 378, 1956.

[27] N. Kroll and J. K. Fassbender: *MEGAFLOW - Numerical Flow Simulation for Aircraft Design.* Springer, 2005.

[28] M. J. Lighthill: *On Sound Generated Aerodynamically. I. General Theory.* Royal Society of London Proceedings Series A, Vol. 211, No. 3, P. 564–587, Maerz 1952.

[29] Kerho M., Heid J., Kramer B. and Ng T.: *Active Drag Reduction Using Selective Low Rate Suction.* AIAA-2000-4018 - 18th AIAA Applied Aerodynamics Conference, 14-17 August 2000, Denver, CO.

[30] P. Moriarty: *NAFNoise: A program for calculating 2D airfoil noise.* tech. rep., National Wind Technology Center, USA, dec 2003.

[31] S. Oerlemans: *Wind Tunnel Aeroacoustic Tests of Six Airfoils for Use on Small Wind Turbines.* tech. rep., NREL, 2004.

[32] S. Oerlemans, P. Sijtsma and B. Méndez López: *Location and quantification of noise sources on a wind turbine.* Journal of Sound and Vibration, Vol. 299, No. 45, P. 869 – 883, 2007.

[33] R. Parchen: *Progress report DRAW, a prediction scheme for trailing-edge noise based on detailed boundary-layer characteristics.* tech. rep., TNO Institute of Applied Physics, The Netherlands, 1998.

[34] J. Park and H. Choi: *Effects of uniform blowing or suction from a spanwise slot on a turbulent boundary layer flow.* Physics of Fluids, Vol. 11, No. 10, P. 3095–3105, 1999.

[35] S. B. Pope: *Turbulent Flows.* Cambridge University Press, September 2000.

[36] Antonia R., Zhu Y. and M. Sokolov: *Effect of concentrated wall suction on a turbulent boundary layer.* Physics of Fluids, Vol. 7, No. 10, P. 2465–2474, oct 1995.

[37] M.C. Remillieux, E.D. Crede, H.E. Camargo, R.A. Burdisso, W.J. Devenport, M. Rasnick, P. Van Seeters and A. Chou: *Calibration and Demonstration of the New Virginia Tech Anechoic Wind Tunnel.* tech. rep., Virginia Polytechnic Institute and State University Blacksburg, Virginia, 2008.

[38] M. Roger and S. Moreau: *Broadband Self Noise from Loaded Fan Blades.* AIAA Journal, Vol. 42, No. 3, P. 536–544, 2004.

[39] Y. Rozenberg, M. Roger and S. Moreau: *Fan Blade Trailing-Edge Noise Prediction Using RANS Simulations.* Acoustical Society of America Journal, Vol. 123, No. 5, P. 3688, 2008.

[40] H. Schlichting, K. Gersten, E. Krause and H.Jr. Oertel: *Boundary-Layer Theory.* Springer-Verlag, 2000.

[41] S. Wagner, R.Bareiss and G. Guidati: *Wind Turbine Noise.* Springer-Verlag, 1996.

[42] A. Wahburn: *A Snapshot of Active Flow Control Research at NASA Langley.* AIAA-2002-3155 - 1st Flow Control Conference, St. Louis, Missouri, June 24-26, 2002.

[43] B. P. Willis and D.O. Davis: *Boundary layer development downstream of a bleed mass flow removal region.* AIAA-1996-3278, ASME, SAE, and ASEE, Joint Propulsion Conference and Exhibit, 32nd, Lake Buena Vista, FL, July 1-3, 1996.

[44] A. Wolf, O. Stalnov, Th. Lutz, W. Würz, S. Seifert and E. Krämer: *Trailing Edge Noise Reduction of Wind Turbine Blades by Active Flow Control.* tech. rep., Institute for Aerodynamics and Gasdynamics, University of Stuttgart, 2010.